21

Electrically Conductive Adhesives

Johann Nicolics and Martin Mündlein

Institute of Sensor and Actuator Systems, Gusshausstraße 27-29, A-1040 Wien, Austria

Abstract

Electrically conductive adhesives are being used in electronic packaging for several decades. A brief review of the dynamic development of conductive adhesives under the influence of the miniaturization, the adaptation of environmental friendly manufacturing processes is presented.

With respect to the importance of isotropically conductive adhesives (ICA), a new contact model to analyze the principle influences of e.g., particle size, particle geometry, and filler content on the percolation threshold is introduced. With this model the arrangement of the particles within a contact is calculated by considering different types of forces (elastic, friction, adhesion, and inertia). Taking into account the electrical properties of the filler particles, the electrical contact behavior including its changes due to aging is investigated.

Finally, typical applications of isotropically conductive adhesives are presented. One example shows how the thermal requirements for attaching a GaAs heterojunction power transistor can be fulfilled using an adhesive with an extremely high filler content (thermal conductivity: >60 W/mK). In another case it is demonstrated how extreme thermomechanical requirements resulting from a thermal expansion mismatch of parts of a sealed IR sensor housing can be corresponded using an adhesive with a comparatively low glass transition temperature. A further example shows a packaging concept of a miniaturized, biocompatible multichip module. For mounting both, narrowly spaced SMDs and bare chips, an isotropically conductive adhesive has been applied.

21.1. INTRODUCTION AND HISTORICAL BACKGROUND

The industrial application of electrically conductive adhesives (ECA) for interconnecting and mounting electronic components on circuit carriers is comparatively new. However, a series of inventions related to various mixtures of conductive and non-conductive substances were made already in the first half of the last century. An early patent of an electrically conductive adhesive describes electromechanical applications already in 1926 [1]. In 1933 Hans Schuhmann claims a *conducting varnish* (consisting of a mixture of about 50% oil varnish, about 40% lithopone, and 10% of soot) which can be applied for shielding purposes in the radio industry [2]. Only two years later it turned out that conducting layers consisting of a binding agent mixed with a finely divided conductor lose their conductivity during operation or do not at all posses this conductivity even if applied in the form in

which they are on the market [3]. In 1944 H.J. Loftis proposed a *molded electrically conductive body* consisting of Bakelite as the resin filled with graphite or metal powder and an additive of an alkaline earth metal salt providing hygroscopic properties to preserve a lubricating effect for the use as commutator brush [4]. An early description of an *electrically conductive adhesive* more similar to the modern ECA can be found in the patent of N.H. Collings et al. in 1948 on the base of a self-setting adhesive and, e.g., finely divided silver powder [5].

The first use of ECAs in electronic technology is known only in 1956: in the U.S. patent [6] *an electrically conducting cement comprising a thermosetting binding medium* is described *for fixing a semi-conducting crystal* (germanium) *to a metal base or holder.* Thereafter, the number of publications reporting experimental and theoretical investigations of electrically conductive adhesives increased continuously. Twenty years later C. Mitchel and H. Berg summarized the state-of-the-art in 1976. They reported that conductive adhesives due to their increasing reliability become more and more acceptable for many different applications. Also the most significant advantages compared to other interconnection techniques, such as low processing temperature and the possibility to use a large variety of low-cost surface fillers are already mentioned [7]. Especially for mounting chips with larger size on substrates with different coefficient of thermal expansion adhesives are superior to eutectic solder alloys due to their significantly higher flexibility. Conductive adhesive bonding started to become popular with the fabrication of plastic-foil keyboards and the use of flexible substrate materials [8].

More recently, in 2000, Alan J. Heeger, Alan G. MacDiarmid and Hideki Shirakawa are awarded the Nobel Prize in Chemistry for their discovery of electrically-conducting polymers whereby initial experiments with silvery shining films of polyacetylene lead back to the beginning of the 1970s [9].

Along with the development of liquid crystal displays (LCDs) in the 80s and their continuing miniaturization a special kind of ECA—the anisotropic conductive adhesive (ACA) has been invented for components with high-lead count and fine pitch interconnections [10,11]. ACAs allow to produce an excellent low-ohmic contact only perpendicular to the mating metalization planes whereby one-particle contact bridges between these metalizations are formed. However, due to their very low loading of conductive filler particles, ACAs remain insulating in the lateral direction. As such, no high-precision printing process is needed. In the meanwhile, ACAs are successfully applied especially for high-resolution displays in portable devices such as notebooks and PDAs (Personal Digital Assistant). Although, the capability of ACAs for comparatively high current load with even up to several Amperes per square millimeter were investigated [12], due to their low filler content their main application fields will probably remain the interconnection of components with low current consumption.

Whereas ACAs have a volume resistivity like an insulator, another type of ECA with a significantly higher degree of conductive filler has a low volume resistivity, comparable with that of conductors (Figure 21.1). They are called isotropic conductive adhesives (ICA, [13]). The goal of this chapter is to develop a deeper understanding of the contact formation process and the influence of application related parameters on the electrical contact resistance of ICAs.

The ICA technology became more interesting in the last years due to several reasons. One of the major driving forces is the increasing packaging density allowing to develop a huge manifold of complex but nevertheless light portable electronic equipments like e.g., cell phones, digital cameras, and notebooks. This development was mainly based on three key factors:

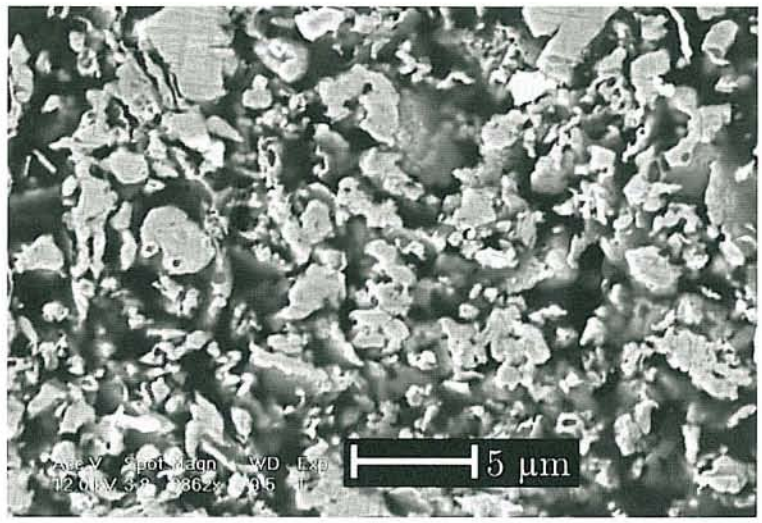

FIGURE 21.1. SEM cross-sectional view of an ICA.

- an inconceivable fineness of structures in the semiconductor level coming close to 0.1 µm and allowing a high integration level,
- a decrease of package size coming down from small outlined (SO) packages over quad flat pack (QFPs), ball-grid arrays (BGAs), and chip-scale packages (CSPs) to direct or bare chip attach techniques like flip-chips (FCs), and
- new printed circuit board manufacturing (PCB) techniques like microvia multilayer technology with plasma or laser structured vias with even less than 0.1 mm diameter allowing to realize a three-dimensional wiring net with extremely high density.

Although, soldering technology has matured through many decades, with the mentioned advances in microelectronics technology a limitation of solder paste become more and more evident in its use for fine pitch components [14]. With current solder paste technology very fine pitch interconnection become hard to handle due to soldering defects such as bridging and solder balling [15–17]. This means to connect the components on the circuit boards under these boundary conditions improved or new interconnection technologies are needed. One of these new techniques could be conductive adhesive bonding. Among these technical demands new legislative reforms make an adaptation of the existing technologies necessary. From the 1st July 2006 on member states of the European Union have to ensure that new electrical and electronic equipment does not contain lead, mercury, cadmium and other named materials. This is regulated in the directive 2002/95/EC of the European Parliament and of the Council on the restriction of the use of certain hazardous substances in electrical and electronic equipment [18]. Under these restriction the prohibition of lead is most serious for the packaging technology because the widely applied solder technology commonly uses solder pastes consisting of a tin lead alloy.

Due to their composition conductive adhesives are innately lead free. Additionally, they allow to avoid flux residues without cleaning. They need a low processing temperature but allow operation at high temperatures. Adhesives are preferable whenever high elasticity is needed to compensate for thermal expansion mismatch between substrate and component body [19–22]. However, compared to soldering, electrically conductive adhesive technology is still in its infancy [23,24]. Two critical issues of conductive adhesives for

surface mount applications are the contact resistance shift during lifetime and a low impact performance [25]. As a long-term effect, the contact resistance of ECAs on ignoble metal finishes can increase dramatically during exposure to elevated temperature and humidity. The low impact performance is observed by separation of components from the board due to impact of significant shock during manufacturing and lifetime of the product. The ability of ECAs to withstand this stress can be determined with the standardized drop test [26]. Another drawback of one-component adhesives compared to soldering is also frequently cited: a lower productivity due to the long curing times. Results obtained by applying a new curing method which allows to reduce the duration of exposition to temperature to an extent comparable to that of soldering processes are also presented.

21.2. CONTACT FORMATION

Let us consider an insulating polymer mixed with a specific amount of conductive particles between a pair of parallel electrodes representing the mating pads of a contact to be formed. It is obvious that these mixture keeps non conductive as long as the particle content is small enough (below its percolation) and the particles are smaller than the gap between the electrodes. If the amount of particles is increased clusters of particles being in contact with each other are formed, whereby the mean size of these clusters increases with the growing amount of particles. From the moment when the first cluster touches both electrodes an electrical connection is formed. If the amount of filler is further increased additional clusters merge successively to one big cluster which leads to an improvement of the electric contact between the two mating pads (Figure 21.2).

The amount of filler particles needed to get the particle-adhesive mixture electrically conductive depends on microscopic geometrical parameters like shape, distribution, and orientation of the particles. The principle influences of these parameters can be analyzed using the percolation theory.

21.2.1. Percolation and Critical Filler Content

The percolation theory is a branch of probability theory dealing with the properties of randomly distributed media in general [27]. One main idea of the percolation theory

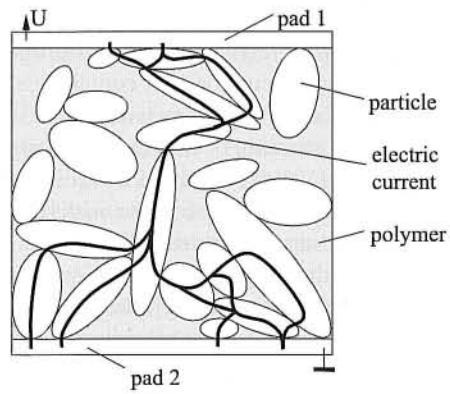

FIGURE 21.2. Schematic cross section of an isotropically conductive joint.

is to predict the macroscopic behavior of a randomly distributed composite material in dependence on its microscopic properties which are expressed purely by statistical data. In case of an isotropically conductive adhesive this composite material is the mixture of the non-conductive polymer and the conductive filler particles. In the simplest case (infinite conductivity of particles and infinite resistivity of the filler) the macroscopic behavior of the joint is described by the probability for a connection path between the two mating pads through the filler particles. Microscopic properties are amount, orientation, shape, size or size distribution of the filler particles. The percolation theory shows that there exists a distinct threshold particle content in excess to which the probability for the formation an *infinite* cluster of particles and therewith for an electrical conductance is bigger than zero and which rapidly increases with rising particle content. This threshold is called the percolation threshold [28].

The percolation theory is valid for infinite systems which means that the particle size is negligible with respect to the distance between the electrodes. Hence, this theory is unable to consider the influence of the particle size on the relation between filler content and percolation probability. However, how important the parameter "particle size" is can be seen by considering an ACA forming a contact with a filler content much below any percolation threshold. In many practical applications of ICAs the relation between the path length (distance between the mating pads in perpendicular direction) and the particle size is only one or two orders of magnitude which causes deviations between ideal (*infinite*) systems as considered by the percolation theory and real ones. For this reason it is important to distinguish between infinite and finite systems. The percolation threshold in an *infinite* system would correspond to the so called *critical filler content* in a real joint. In real (= *finite*) systems only clusters with a limited number of particles are necessary for an electrical connection between the mating borders. The smaller a contract system with respect to the particle size the mellower is the transition between the non conductive and the conductive state in the percolation curve or more precisely: in the conduction probability-versus-filler content function (a comparison with the ideal percolation curve can be seen in Figure 21.5). Nevertheless, here the terminology *percolation curve* is used defining the *percolation threshold* as the point on which the probability of an interconnection is 50% for real systems. (For definitions, symbols and terminology used in this chapter refer to the Section Notations and Definitions.)

21.2.2. ICA Contact Model

Using the percolation theory, it is possible to show principle influences on the properties of isotropically conductive adhesives depending on the geometric properties of the particles. But in order to get a deeper understanding of the processes inside a conductive adhesive joint additional factors have to be considered. Such factors are the volume electrical conductance of the filler particles, the contact resistance between the particles, and the particles and the pads, the influence of surface films on the contact resistance, the mechanical force between the particles, and the effects of oxidation and galvanic corrosion on the electric resistance of the joint [29].

For this purpose, a two-dimensional (2D) model of a complete joint including a numeric simulation was developed which is capable of calculating the particle alignment and density distribution as well as the voltage and current distribution inside the model area. On this base the total DC-resistance of the modeled joint was calculated. The model is based on the following considerations and assumptions [30]:

- the modeled system is two-dimensional,
- the considered area is rectangular,
- the pads are on the top and on the bottom borders of the model area,
- the conductivity of the polymer is neglected,
- the particles have elliptic shape with arbitrary aspect ratio (length ratio of major to minor axes),
- the particles may initially have an arbitrary orientation and can overlap whereby the condition for the final orientation and position of the particles is found by a simulation of the particles' alignment as described below by the assumption that the size of the overlapping area is directly related to a repulsion force between the particles.

A 2D simulation of a percolation problem shows a systematic difference to the three-dimensional (3D) problem. In a 2D percolation the threshold is shifted to higher filler contents. In the case of an ICA this can be observed by an increase of the contact resistance when the thickness of an adhesive layer is reduced [31–33]. Despite of this fundamental difference between the 2D and 3D model the percolation theory shows that the principle behavior of a random particle network obeys the same rules [34]. This means the absolute values derived from the 2D do not directly correspond to the 3D case but show the analog dependencies on the particle parameters like shape, orientation or distribution. However, the computational effort can be reduced drastically for a 2D numerical simulation and the computing capacity saved in this way can be used to investigate a higher number of different dependencies. For this reason, the presented simulation is restricted to the 2D case and can consider the change of size of the contact areas at the mating surfaces of the particles in dependence of the contact force. Moreover, the simulation considers the dependency of the contact resistance on particle shape, particle orientation, etc.

21.2.2.1. Simulation of the Particles' Alignment The simulation is capable of establishing the geometrical alignment of the elliptical particles based on mechanical effects like inertia, conservation of momentum, Hooke's law, and friction. This method is known as discrete element modeling (DEM) which is an explicit numerical method where individual separate elements (particles) react with their neighbors by their contact areas through friction and adhesion (DEM was first applied by Peter Cundall in 1971 to geotechnical and granular flow problems [35]).

For each time step an overlapping between the particles at their contact points is assumed in order to consider a pressure-dependent deformation of the particles. Figure 21.3 illustrates the forces of one particle in a non-equilibrium calculation step. The considered particle is in contact with another one and the upper pad. Elastic forces F_{e1} and F_{e2} are defined as functions of the size of the respective overlapping area whereby the direction of these forces is perpendicular to the chord between the intersection points S_{1a}, S_{1b}, S_{2a}, S_{2b}.

In order to define an electrical contact resistance between neighboring particles a contact force between them has to be present. In an ICA these contact forces are assumed to result from shrinking of the polymer during the curing process and have to be considered in order to simulate the DC-resistance of an ICA joint [36,37]. For this reason, an attracting force F_a between intersecting particles resulting from the compaction of the particle network during the curing of the polymer is introduced. The direction of this attracting force is antiparallel to the respective elastic force. The norm is proportional to the length of the chord between the intersecting points.

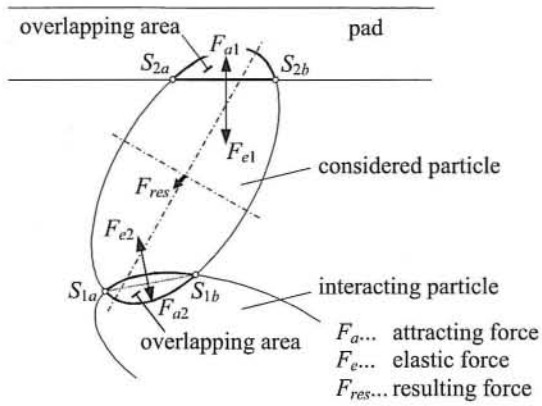

FIGURE 21.3. Schematic illustration of the overlapping area between adjacent particles, and mechanical forces leading to a rearrangement of the particles.

For each particle these attracting and repulsing elastic forces at different contact points can be added-up to one resulting force F_{Res} which causes a rearrangement. This rearrangement motion of the particles is controlled by inertia, a damping force and a friction force. Similarly, the resulting torsional moments are calculated for each particle. The distribution of the resulting rearrangement forces and moments are successively optimized in a looped calculation procedure leading to the final particle arrangement. Depending on the relation between the attracting force and the elastic force a defined overlapping between the particles remains at the equilibrium state.

21.2.2.2. Simulation of the Total Joint Resistance After the particle alignment is being calculated the electric resistance of the joint is simulated. This is done in several steps. The first step is to separate each single particle from the base model, whereby the voltage distribution inside the respective particle is calculated using a finite difference method [38]. As boundary condition, the potentials of the contact areas to the neighboring particles are defined. When the voltage distribution is calculated for $n-1$ different sets of boundary conditions it is possible to calculate an admittance matrix describing the particle as $(n+1)$-pole, where n denotes the number of neighbored particles. (The $(n+1)$ pole as an additional pole located in the particle center is introduced for simplifying indexing and set-up of the equation system.) This idea is depicted in Figures 21.4(a) and (b).

After an admittance matrix is being calculated for every particle, the resulting $(n+1)$-poles are connected to one network which contains the information on the particle distribution of the entire joint including the pad arrangement. The effort for calculating the contact resistance to the required extent is reduced by excluding particles which do not contribute to the current transportation from the network. In order to model more realistic contact properties a transition resistance between the particles is taken into account. For this purpose, additional resistors (R_{pp} and R_{ppad}) between the respective connections of the $(n+1)$-poles are introduced [Figure 21.4(c)]. The value of each individual transition resistance depends on the contact force which controls the size of the overlapping area. As a measure for the size of the overlapping area and therewith for the contact resistance between the two considered particles the length of the intersection line (e.g., $w_s = \overline{S_{1a}S_{1b}}$ in Figure 21.3) is used. The interface conductivity between two particles is then obtained as product of a normalized specific conductivity λ_{pp} and the length of the intersection line w_s

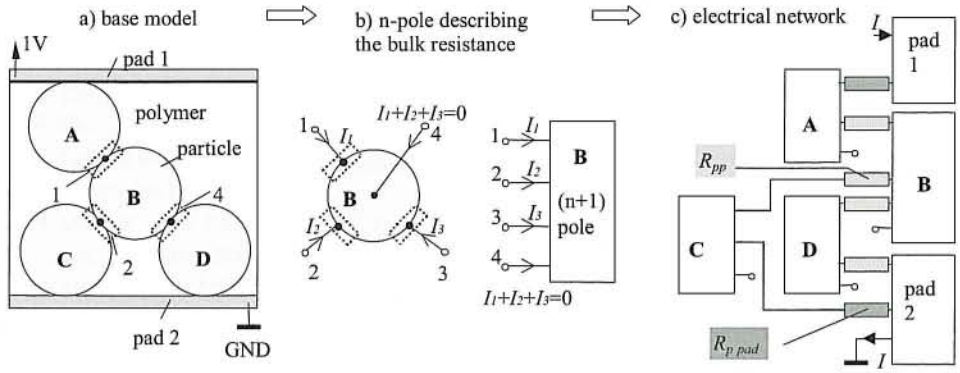

FIGURE 21.4. Basic principle for calculating the electric resistance.

of the involved particles. In turn, the normalized interface resistance R_{pp} between two particles or $R_{p\,pad}$ between a particle and a pad are calculated according to following relation, respectively:

$$R_{pp} = \frac{1}{\lambda_{pp} \cdot w_s} \quad \text{or} \quad R_{p\,pad} = \frac{1}{\lambda_{p\,pad} \cdot w_s}. \tag{21.1}$$

As final step the equations of this network are solved. Thereafter, the potential at each contact point is found and the total joint resistance is calculated.

21.2.3. Results

21.2.3.1. Percolation Behavior The established model allows us to analyze different fundamental properties of conductive adhesive joints. In the first step, only the percolation behavior is investigated. For this purpose, only the particle alignment is calculated and the probability of an interconnection p_p from one pad to the other is determined as a function of the filler content ϕ in % of area. For all simulations, a quadratic model area with a normalized edge length of 1 is chosen. Figure 21.5 shows the dependence of p_p for circular particles with different diameters d. It can be seen that the slope of the curve decreases for larger diameters in accordance with the theory. In the literature for the case of *hard-core* circles (neighboring particles only touch at one point), a critical filler content ϕ_c lies between 0.45 and 0.55 [34].

In Figure 21.5 the results of the simulation with the percolation theory is compared. At an interconnection probability of $p_p = p_c \equiv 0.5$ (which is defined as the percolation threshold for the finite system) the simulation provides filler content values of ϕ_c between 0.55 and 0.57. For the smaller particles the higher values are valid. The smaller the particles are, the more the infinite system is approached (which is described exactly by the percolation probability).

A further fact in this model is the deformability of the particles which corresponds to a combination of the *hard-core* and the *soft-core* model where the particles may touch along a line (not just a point) due to arbitrary overlapping. In the literature one can find the value $\phi_c = 0.68$ for the *soft-core* circles system [39].

In an ICA joint the electrical conductance is provided by the conductive particles, and the mechanical strength derives only from the polymer. This means: to preserve the

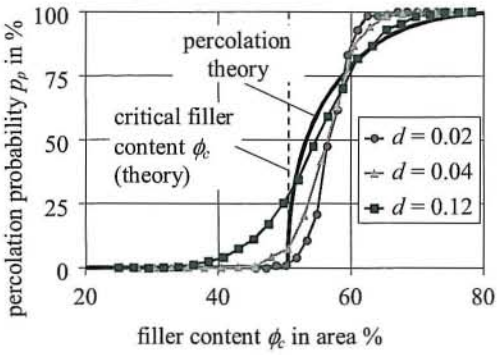

FIGURE 21.5. Comparison of percolation probability and probability of interconnection with circular particles as a function of the filler content.

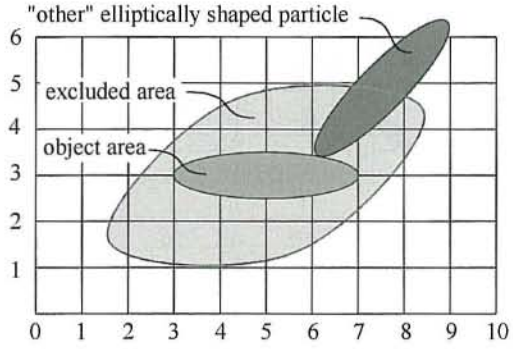

FIGURE 21.6. Excluded area for ellipses with the same shape but different orientation.

mechanical stability of the joint the particle content has to be as small as possible. This can be obtained with highly elongated particles like flakes, sticks, or tubes. However, for non-circular particles, a given filler content will lead to a different interconnection probability. In order to understand the influence of the particle shape on the filler content area which is necessary to obtain e.g., the 50% threshold to form an interconnection it is helpful to start at the definition of the so called *excluded volume* which is reduced to the *excluded area* in the two-dimensional case. The excluded area A_{ex} of an object (particle) is defined as the object area itself plus the area around this object into which the center of another similar object is not allowed to enter if overlapping of these two objects is to be avoided [34]. For example, for circles with the radius r the excluded area A_{ex} is $4r^2\pi$. For two ellipses of the same shape but different (constant) orientation the excluded area is shown in Figure 21.6. From a heuristic consideration it becomes obvious that the percolation threshold is lowered if the excluded volume is increased.

The excluded area is increased when circular particles are stretched to ellipses. The bigger the aspect ratio at a constant particle area the bigger is the excluded area. This tendency is shown in Figure 21.7 where three cases of excluded areas are formed with two ellipses of the same shape and size (relation between major and minor axis $X = 16$), respectively, but different mutual orientation ($\delta = 0°$, $\delta = 45°$, and $\delta = 90°$). One can see that the excluded area increases significantly with rising angle δ. The maximum possible value of the excluded area also depends on the shape of the particles. Figure 21.8 depicts

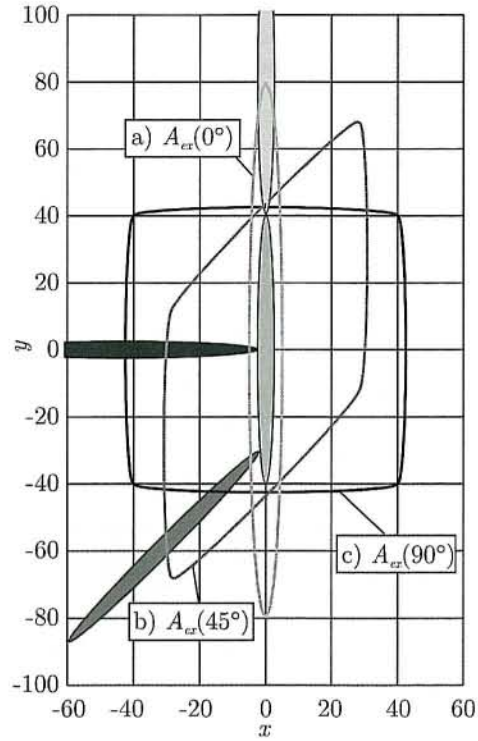

FIGURE 21.7. Comparison of three cases of excluded area for equal ellipses but different orientation: (a) $\delta = 0°$, $A_{ex} = 4 \cdot A$, (b) $\delta = 45°$, $A_{ex} = 16.5 \cdot A$, (c) $\delta = 90°$, $A_{ex} = 22.5 \cdot A$; relation between length of major and minor axis of ellipses $X = 16$.

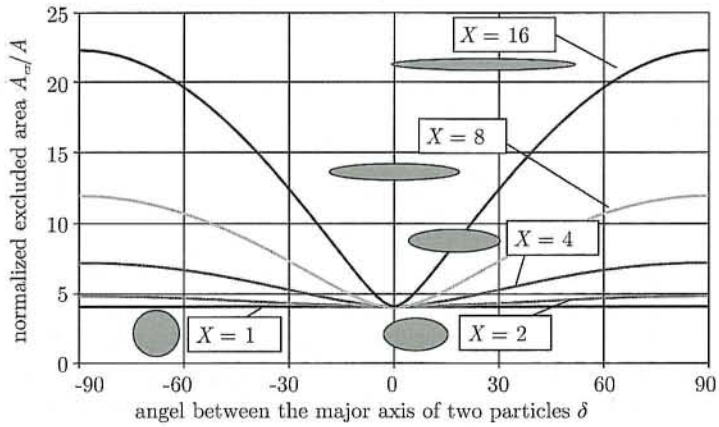

FIGURE 21.8. Normalized excluded area versus angle δ between elliptic particles with various aspect ratios ($1 \leq X \leq 16$).

the normalized excluded area versus angle δ between elliptic particles with various aspect ratios ($1 \leq X \leq 16$). It should be noted that the dependence of the excluded area on the orientation of the particles with respect to each other becomes stronger the more oblong the particles are.

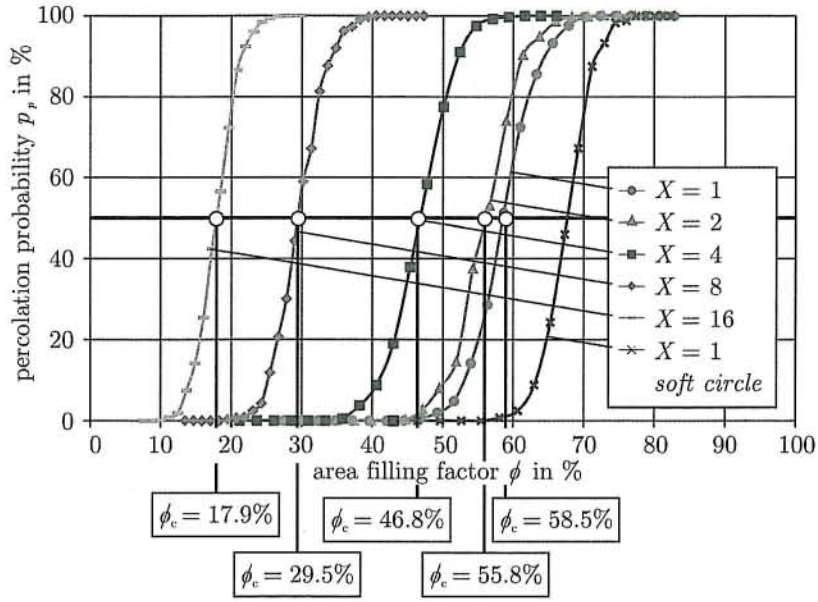

FIGURE 21.9. Probability of interconnection as a function of the filler content for elliptic particles with the same area but different aspect ratio.

The influence of the excluded area on the percolation behavior can be recognized in Figure 21.9 where the percolation probability p_p for elliptical particles with different aspect ratio is depicted as function of the filler content ϕ. It can clearly be seen the decreasing critical filler content (the respective filler content at a probability level of 50%) with the increasing aspect ratio of the particles. All particles in Figure 21.9 have the same area as a circular particle with the diameter $d = 0.04$.

A further important parameter is the mean number B of neighboring particles. With increasing filler content the number of particles being in contact with each other grows. On reaching the percolation threshold the following relation is valid:

$$B_c = \phi_c \frac{\langle A_{ex} \rangle}{\langle A \rangle}, \tag{21.2}$$

where B_c is the critical mean number of neighboring particles, $\langle A \rangle$ is the mean particle area, and $\langle A_{ex} \rangle$ is the mean excluded area. For circular particles B_c varies in the range between 1.8 and 2.2 [34]. One can expect that this range should also be valid for elliptically shaped particles. However, the values of ϕ_c obtained from the simulation described here are consistently some percent bigger than those from the percolation theory. These differences derive from two factors: One as already mentioned above is that the percolation threshold derived from the percolation theory is defined differently as ϕ_c. The relation between the particles' size and the ICA layer thickness is considered in the simulation more realistically as a finite value which means that p_p is always higher than the theoretical percolation probability. The second factor is that a contact force was introduced in this model which equalizes the contraction forces (e.g., from the cured polymer binder) by a variable overlapping area between the particles. This leads to an increased mean value of neighboring particles B_c and changes the system in direction to the soft core model. Moreover, B_c also

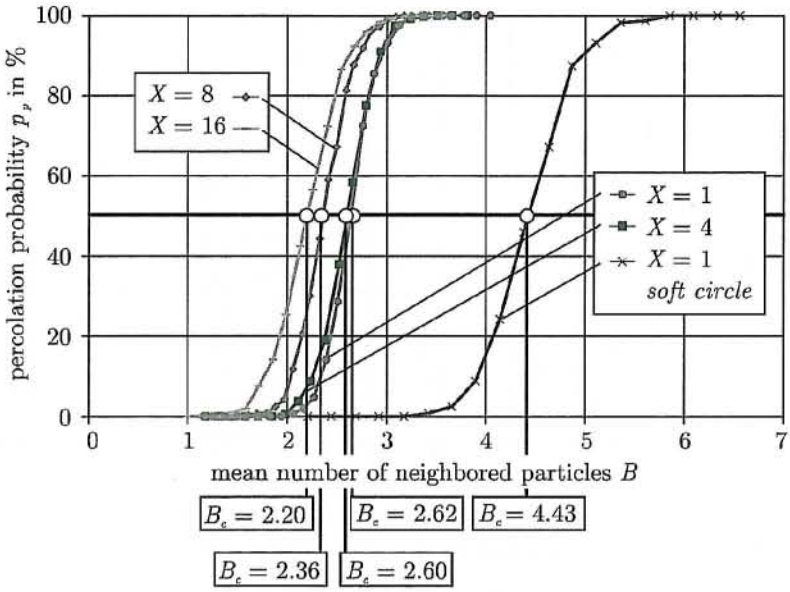

FIGURE 21.10. Percolation probability p_p versus the number of neighbor particles B for elliptical particles with different various aspect ratios ($1 \leq X \leq 16$).

varies with the particle geometry as can be seen in Figure 21.10 depicting the percolation probability versus the number of neighbor particles for elliptical particles with various aspect ratios ($1 \leq X \leq 16$). The diagram demonstrates that a higher number of neighboring particles with circular than with oblong form is needed to obtain the same percolation probability. For comparison, in Figure 21.10 the respective curve for soft circular particles is also displayed. In this case $B_c = 4.43$ which agrees with the respective value reported from Balberg et al. [34]. This comparison allows to understand the fundamental difference between *hard-core* and *soft-core* model.

Typical particle arrangements for illustration of the influence of the particle geometry on the respective filler content necessary to obtain an electrical connection between the pads are depicted in Figure 21.11. The particles have all the same area and in all cases the percolation probability is 50% ($\phi = \phi_c$). However, only arrangements are selected which provide at least one electrical connection between the mating pads. Particles contributing to an electrical path are displayed dark whereas the light particles are isolated or are linked to clusters which have electrical contact at most with only one pad.

In all subpictures it is conspicuous that only a comparatively small percentage of particles is involved in the current transportation. Frequently the current path is necked to a single chain of particles. This fact is directly related to the condition of a percolation probability far below 100%. The electrical consequences are discussed more thoroughly in the next subsection. In particular a strong dependence of the critical filler content on the particle geometry becomes obvious: ϕ_c varies from almost 55% for circular particles to less than 21% for elliptical particles with an aspect ratio of $X = 16$.

Until now we have considered the percolation probability under the condition that the particles may have an arbitrary orientation, i.e., δ was uniformly distributed in the interval from $-90°$ to $+90°$. However, oblong particles like silver flakes in an epoxy adhesive (in order to consider an example of the system most important for practical applications) may

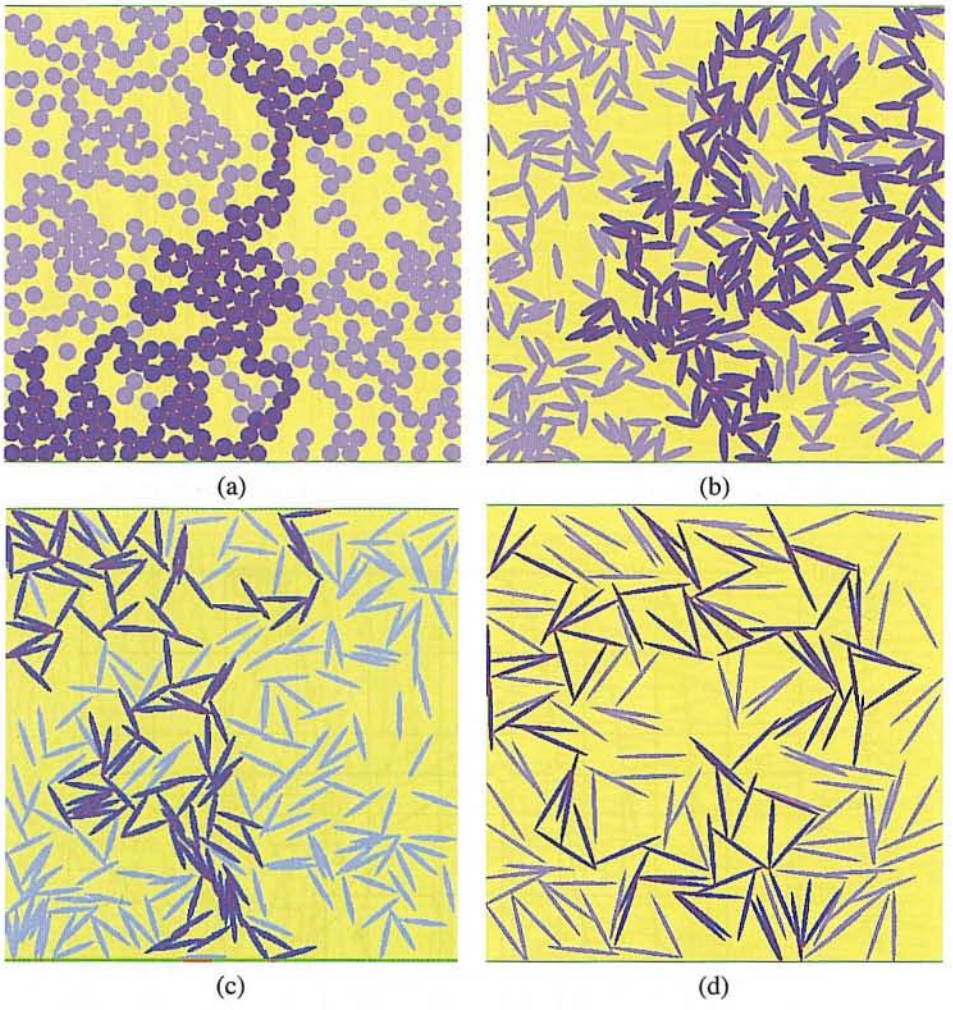

FIGURE 21.11. Particle arrangements with various filler content and various aspect ratio characterized by a percolation probability of 50%, respectively (all particles have the same area). (a) 445 particles, axis ratio 1, filler content 54.5%. (b) 380 particles, axis ratio 4, filler content 46.0%. (c) 255 particles, axis ratio 8, filler content 30.5%. (d) 170 particles, axis ratio 16, filler content 20.8%.

underlay constraints e.g., in the vicinity of the plane contact pads which, to some extent, force a parallel alignment of the particles as can be observed in microsections of ICA bonds. Therefore, a more realistic model should consider these constraints by limiting the freedom of orientation. In Figure 21.12 the effect of different degrees of freedom on the mean normalized excluded area $\langle A_{ex} \rangle$ is demonstrated. A restriction of the orientation to e.g., $-30° \leq \delta \leq +30°$ leads to a reduction of $\langle A_{ex} \rangle$ to about the half of the value for the unlimited freedom of orientation ($-90° \leq \delta \leq +90°$). If all particles are parallel ($\delta \approx 0$) the minimum of $\langle A_{ex} \rangle = 4$ is obtained. The practical meaning of this consideration is, that a higher filler content is needed in cases of a limited freedom of particle orientation.

Whereas in an infinite system the influence of the contact pads on the orientation of the particle does not exist, in the considered limited system this influence plays an impor-

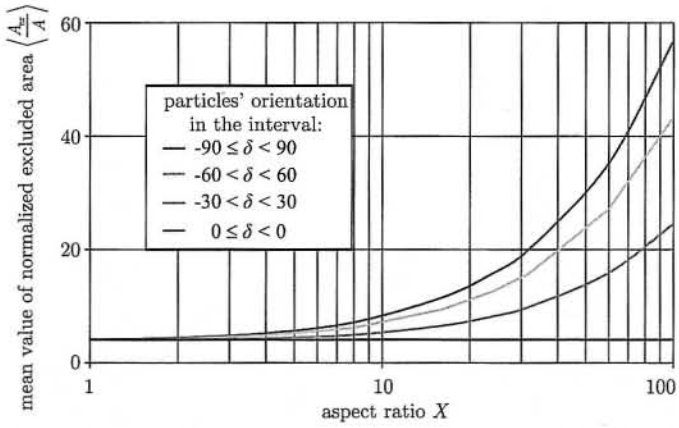

FIGURE 21.12. Mean normalized excluded area $\langle A_{ex} \rangle$ versus aspect ratio for different limitation degrees of possible particle orientation. Within the respective intervals δ is assumed to be uniformly distributed.

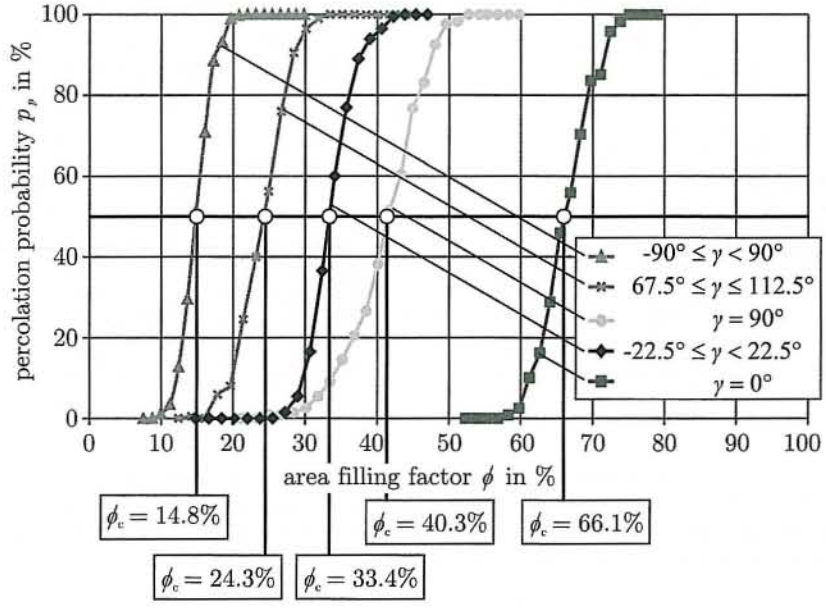

FIGURE 21.13. Percolation probability as function of the filler content for two cases of limited freedom of particle orientation ($\gamma = 0°$ and $\gamma = 90°$) and three different ranges of freedom (γ within $\pm 22.5°$ to the horizontal axis, $\pm 22.5°$ to the vertical axis, and no restriction: $-90° \le \gamma \le 90°$).

tant role. From a heuristic consideration one may expect a lower required filler content if the particles are oriented perpendicular to the pad surfaces. In order to analyze the influence of the particle orientation with respect to the contact pads the angle γ between the long particle axis and the pad plane (horizontal in this case) is introduced. The highest filler content is needed if all particles are aligned parallel to the pad plane ($\gamma = 0°$). On a first glance one could expect the lowest critical filler degree ϕ_c in the case when all particles are oriented perpendicular ($\gamma = 90°$). However, this is not the case. An analysis of the

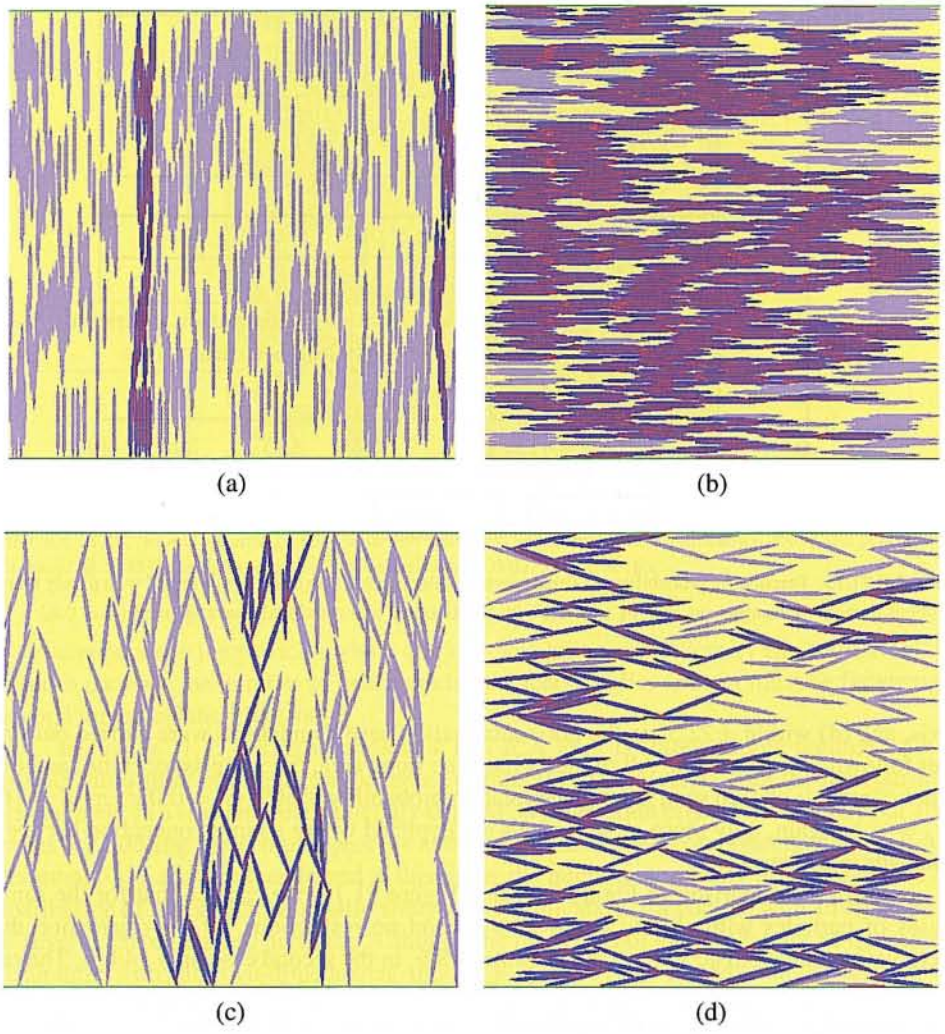

FIGURE 21.14. Accidental particle arrangements for different conditions (a) $\gamma = 90°$, (b) $\gamma = 0°$, (c) γ within $\pm 22.5°$ to the vertical axis, and (d) $\pm 22.5°$ to the horizontal axis. All particles have the same area ($0.02^2 \cdot \pi$), the same aspect ratio $X = 16$, the percolation probability is 50%. Particles contribution to the interconnection between the pads are displayed in dark color. (a) 365 particles, $\gamma = 90°$, filler content 41.6%. (b) 609 particles, $\gamma = 0°$, filler content 66.1%. (c) 199 particles, $67.5° \leq \gamma \leq 112.5°$, filler content 24.2%. (d) 279 particles, $-22.5° \leq \gamma \leq +22.5°$, filler content 33.3%.

percolation probability as function of the filler content clearly shows a lower critical filler content in cases when the particle orientation may vary to some extent (γ within $\pm 22.5°$ to the horizontal axis, $\pm 22.5°$ to the vertical axis, and no restriction: $-90° \leq \gamma \leq +90°$) compared to cases without any freedom ($\gamma = 0°$ and $\gamma = 90°$, Figure 21.13). The lowest possible critical filler content ϕ_c is again reached with an unlimited fan out of the particle orientation.

The role of the particle orientation for the percolation probability is visualized in Figure 21.14 along with four accidental particle arrangements as calculated by this simulation for the different conditions (a) $\gamma = 90°$, (b) $\gamma = 0°$, (c) γ within $\pm 22.5°$ to the vertical

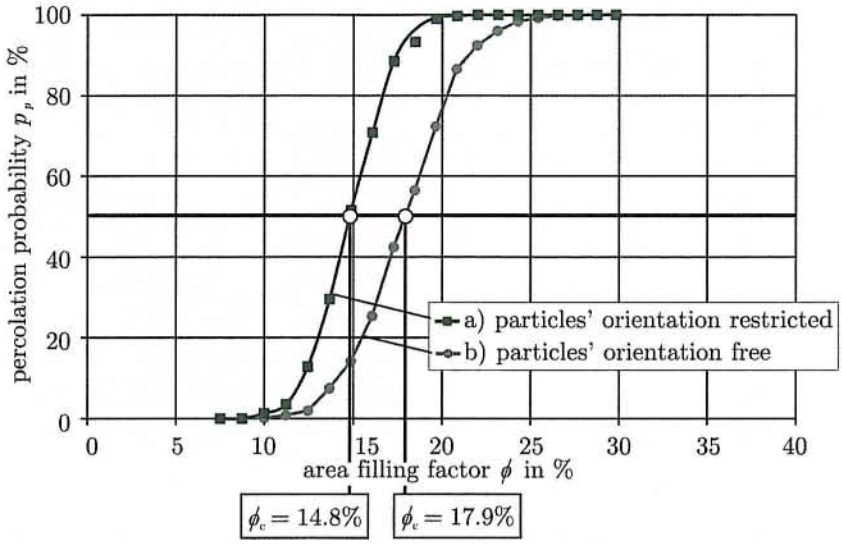

FIGURE 21.15. Percolation probability p_p versus particle filler content ϕ in case of (a) a model with purely translational particle rearrangement and (b) a model with translational and rotational rearrangement ($A = 0.02^2 \cdot \pi$, $X = 16$).

axis, and (d) within $\pm 22.5°$ to the horizontal axis. These simulations were carried out under following assumptions: All particles have the same area, the same aspect ratio, and the filler content is chosen such that the percolation probability is 50% ($A = 0.02^2 \cdot \pi$, $X = 16$, $p_p = p_c$). Again, only those arrangements are depicted where an interconnection between the pads is achieved.

From a comparison of Figure 21.9 and Figure 21.13 one can see that for the same cases of particles with elliptic shape $X = 16$ and no restrictions for the orientation the percolation threshold ϕ_c in one case is almost 18%, in the second case only 14.8%. The respective curves are shown in Figure 21.15. The difference of 3.2% results from the fact that the simulation of the particle arrangement has been carried out in different ways: In the first case the simulation started with the placement of particles with randomly and uniformly distributed orientation and only translational movements were allowed for the rearrangement of the particles. In this way the equidistribution of the orientation was constrained. By contrast, in case of the left curve of Figure 21.15 after placement of the particles besides the translational also a rotational rearrangement was permitted. These rotations allow the particles to increase the extent of parallel orientation of neighbored particles. This effect can counteract against the equidistribution of the orientation and in turn lead to an increase of the percolation threshold. The more the filler content is increased the more significant becomes this effect of paralleling of particles. This effect is clearly visible in Figure 21.16 showing a model with 400 particles being allowed to rotate after their placement. Due to the comparatively high filling degree of $\phi = 45\%$ a high degree of parallel clustering can be observed. Another aspect can also be recognized from this figure: not only the total number but also the percentage of electrically active particles (dark colored) is increased significantly when the percolation probability exceeds the threshold value. The number of parallel current paths per unit of contact area is of great practical importance for joints with high current loads. It must be noted that in any case the current is necked to the microscopic

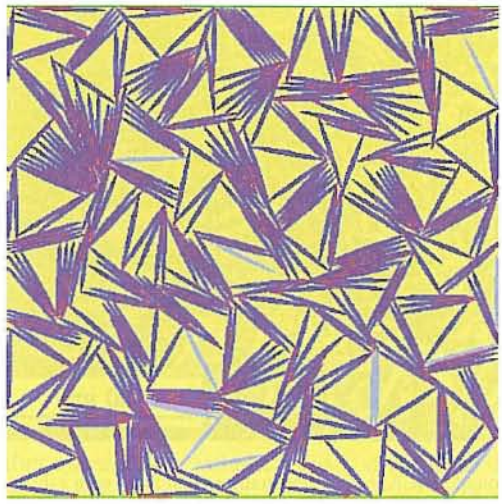

FIGURE 21.16. Model of arrangement with 400 particles. A filler content significantly above the percolation threshold ($\phi = 45\%$) leads to paralleling of particles ($A = 0.02^2 \cdot \pi$, $X = 16$).

interfaces between the particles where an extremely high current density can be reached. In order to increase the number of interparticle contacts the filler content must be far enough beyond the percolation threshold.

In Figure 21.17 a microsection of a real ICA joint is shown. Some regimes with a distinct uniformity of orientation becomes visible. It can be assumed that the final particle arrangement in a real joint does not only depend on production process parameters but also varies e.g., during the printing process and during placing the components due to plastic deformation. As can be recognized in this figure the microhomogeneity is not ensured. The distribution of the particle orientation may vary significantly in a volume with an elongation of several ten to hundred particles. Although the properties of an ICA cannot be quantified accurately with this two-dimensional model, it just provides a deeper understanding of some phenomena and can be used to predict tendencies. The next section deals with the investigation of electric joint properties on the base of simulated particle arrangements.

21.2.3.2. Joint Resistance For a reliable isotropically conductive adhesive joint the percolation probability has to be 100%. In the simulation this means in the case of elliptical particles with an axis ratio of $X = 4$ a filler content of >60% is needed. In order to establish the percolation probability p_p and the average value of the total joint resistance as functions of the filler content ϕ, 600 simulations with accidental starting condition and identical parameters (but different particle arrangements) were performed for every ϕ value. Results are shown in Figure 21.18. In order to get the resistance curve also for filler contents below a percolation probability of 100% it was necessary to exclude particle arrangements without electrical connection between the contact pads from this consideration, since they would have led to an infinite resistance. However, the lowered number of evaluable simulation results is related to an increase of uncertainty in the resistance calculation which causes widening of the average deviation of the resistance curve.

For simplicity, in a first approximation the contact resistance between the particles is assumed to be zero (ideal contact) and the bulk conductivity σ_{pad} of the two pads is assumed to be 1000 times that of the particles' one ($\sigma_{pad} = 1000 \cdot \sigma$) so that the potential

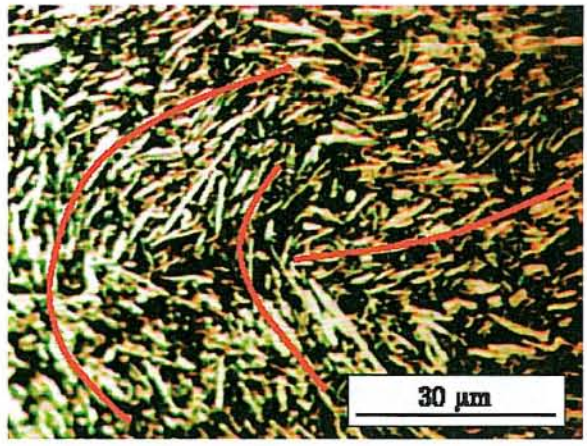

FIGURE 21.17. Microsection of an ICA joint demonstrating small areas with a distinct uniformity of orientation (along red lines). An orientation structure becomes visible.

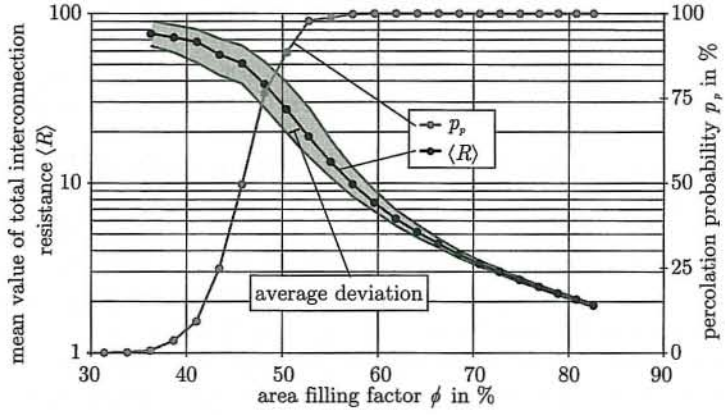

FIGURE 21.18. Probability of interconnection and the average joint resistance versus the filler content (elliptic particles with an axis ratio of $X = 4$).

in the pads can be considered as constant and the total joint resistance depends only on the particle resistance. In order to receive results which are independent from the system size a specific conductivity of the particles of $\sigma = 1$ is introduced. For the calculation of the joint resistance this means: If the quadratic model area would be completely filled with particle material ($\phi = 100\%$) the joint resistance would be 1. At a more realistic filler content of 77% the joint resistance reaches a value of 2.6. In the simulation the first contact occurred at $\phi = 38\%$ leading to a considerably higher joint resistance of 67. In between these two points, at $\phi = 60\%$, the interconnection probability just reaches the 100% value. At this level the normalized total joint resistance amounts 9.4. This shows that the major change of the contact resistance occurs in a range where the percolation probability is below 100%. By increasing the filler content above this point a strongly decreasing width of the average deviation of the joint resistance R can be observed indicating a regime of reliable interconnection.

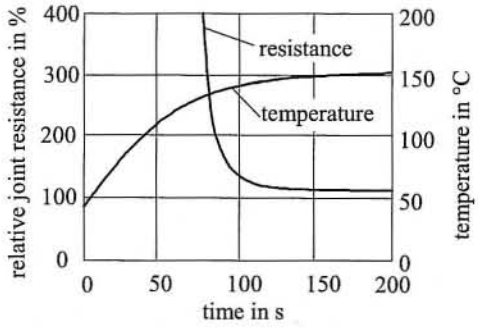

FIGURE 21.19. Change of the joint resistance during curing process.

Although, the filler content as a volume ratio is difficult to compare with that of a two-dimensional model, from a microsectional view of a real ICA joint one would obtain a value ϕ far beyond 60% which means definitely an interconnection probability of 100%. Nevertheless, an ICA just after being dispensed or printed on a substrate behaves like an insulator. The low joint resistance corresponding to an interconnection probability of 100% arises only successively during the curing process. In Figure 21.19 such a break-down of the joint resistance at the beginning of the curing process is depicted. This phenomenon is based on a strongly changing contact resistance R_{pp} between the particles which are brought into an intimate contact during the development of the contraction forces of the polymer binder as described in Section 21.2.2. It can be considered in this model e.g., by introducing a time and temperature dependent function describing the effect of the curing process. Such a simulation shows that the interface resistance between the particles and certainly also between particles and pads are the most significant parameters for modeling an ICA joint. In order to take into account different interface effects like corrosion at the pad-particle interfaces or oxidation between particles, both effects known as aging phenomena, the specific interface conductivity λ_{pp} between two particles and λ_{ppad} between particle and pad are introduced.

By contrast to Figure 21.18 where all transition resistances at interfaces where neglected let us assume the more realistic case of a finite conductivity at the interfaces. Taking the same particle arrangement but values of λ_{pp} and λ_{ppad} between 1 and 0.001 one can observe that in a logarithmic scale the total joint resistance as functions of the filler content have the same shape but are shifted to higher $\langle R \rangle$ values. This means that the effect of a change of transition conductivity is almost the same at any degree of filler. How strong this effect is, depends on the relation between the conductivity of the particles and their interfaces. The lesser the interface conductivity is, the more it controls the total joint resistance.

By keeping the interface conductivity between the particles constant at $\lambda_{pp} = 1$ and varying the one between particles and pad dependencies of the total joint resistance on ϕ are obtained (Figure 21.21). This corresponds to the practical case of a joint degradation e.g., due to galvanic corrosion at the interface between metalization and ICA.

It can be recognized that now the effect of λ_{ppad} on the total joint resistance is much weaker than in the case when $\lambda_{pp} = \lambda_{ppad}$ (Figure 21.20). A change of interface conductivity λ_{ppad} does not appear any more as resistance multiplier but rather acts as a supplement to the resistance of the ICA fill. This becomes clearer by considering the pad surfaces as equipontential planes and by defining a total transition resistance $\langle R_{tr} \rangle$ consisting of inter-

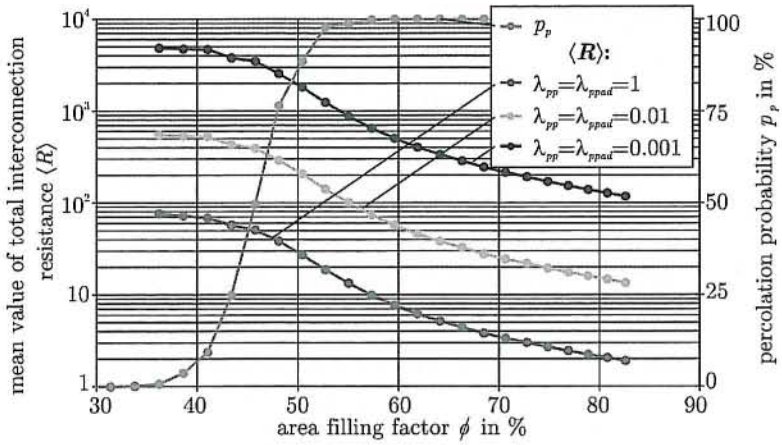

FIGURE 21.20. Normalized total joint resistance and percolation probability versus filler content for various values of normalized interface conductivity under the condition of $\lambda_{pp} = \lambda_{ppad}$.

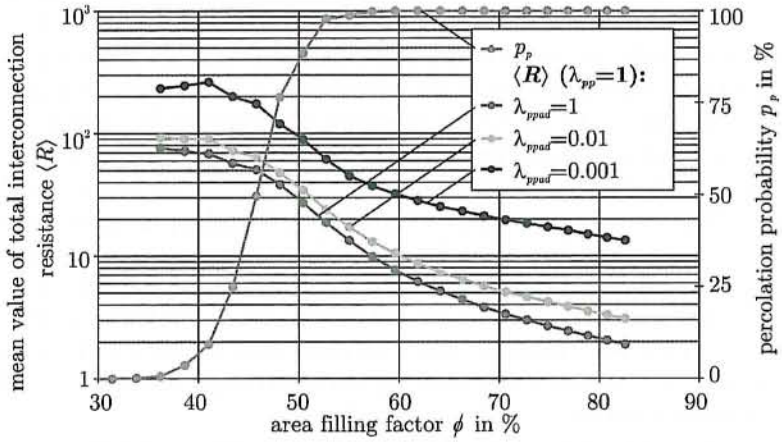

FIGURE 21.21. Normalized total joint resistance like in Figure 21.20 but for constant normalized particles' interface conductivity ($\lambda_{pp} = 1$).

face resistances of only those n particles touching the pad which are also involved in the current path according to the following relation:

$$\langle R_{tr} \rangle = \frac{1}{\sum_i^n \lambda_{ppad} \cdot w_{s,i}} = \frac{1}{\lambda_{ppad}} \cdot \frac{1}{\sum_i^n w_{s,i}}, \tag{21.3}$$

where $w_{s,i}$ is the length of the intersection line of the ith particle. The sum

$$w_s^* = \sum_i^n w_{s,i} \tag{21.4}$$

of all these lengths can be understood as *effective contact length* to which the current is necked at the respective pad interface. The total pad interface resistance is the sum of both

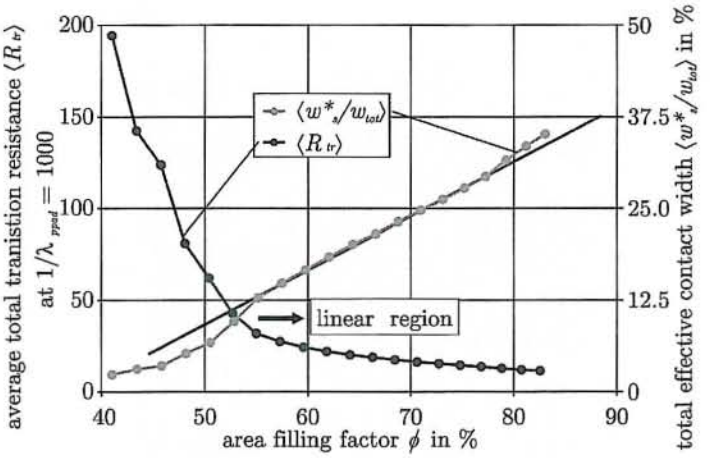

FIGURE 21.22. Total transition resistance at both pad-particle interfaces and normalized effective contact length as functions of the filler content.

interface effects (which are equal for both pads in this case but one could consider different interfaces as well):

$$\langle R_{tr} \rangle = \frac{2}{\lambda_{p\,pad} \cdot w_s^*}. \tag{21.5}$$

This resistance can again be calculated as function from the filler content. A comparison with the results depicted in Figure 21.20 shows that it corresponds very well to the difference of the total joint resistance functions of the two cases $\lambda_{pp} = \lambda_{p\,pad} = 1$ and $\lambda_{pp} = \lambda_{p\,pad} = 0.001$. This is illustrated by Figure 21.22. This diagram also shows that the average effective contact width normalized to the total width w_{tot} of the modeled space demonstrates a linear increase with the filler content in a wide regime above the 100% percolation threshold. In Figure 21.23 the particle arrangement of a model with 70% filler content is depicted where the effective contact length amounts around 25% of the total model width.

For practical applications it is important to note that there is a distinct decrease of the interfacial resistance with increasing filler content. One could expect an improvement of quality of an ICA joint with rising filler content. However, in this case the bonding forces resulting from the adhesion of the polymer to the pad surface are reduced to the complement part of the effective contact area. This consideration allows to understand that a compromise between high mechanical strength and low total joint resistance has to be found which depends on the respective application field.

A further parameter influencing the joint resistance is the particle shape, since this is a controlling parameter of the percolation behavior as discussed before. For this purpose the joint resistance for various aspect ratios of elliptic particles is investigated. Figure 21.24 shows the results for the cases $X = 8$, $X = 4$, and circular particles, when $\lambda_{pp} = \lambda_{p\,pad} = 1$. The results clearly show qualitatively similar dependencies versus the filler content whereby the critical filler content is shifted in almost equal steps from 30%

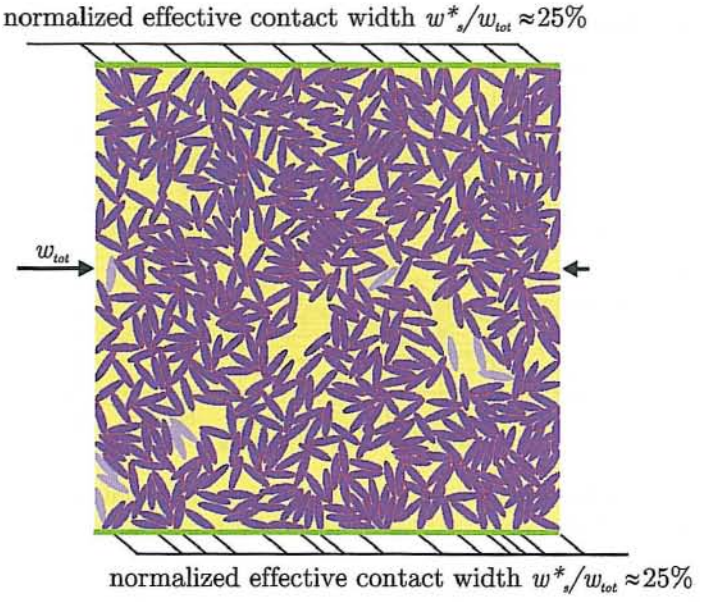

FIGURE 21.23. Particle arrangement of a model with 70% filler content providing a relation of around 25% effective contact width to total model width.

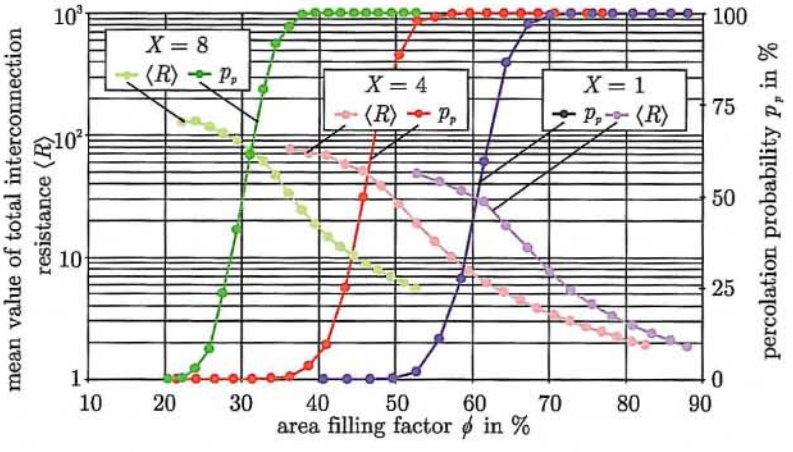

FIGURE 21.24. Total joint resistance and percolation probability versus filler content for particles with various aspect ratios.

for the oblong particles to around 60% for the circular ones. This comes out clearer by introducing the deviation $\Delta\phi$ of the filler factor ϕ from critical value ϕ_c as

$$\Delta\phi = \phi - \phi_c. \tag{21.6}$$

This transformation shifts the results of Figure 21.24 such that the point of percolation remains the same for all three cases and shows that also the minimum additional

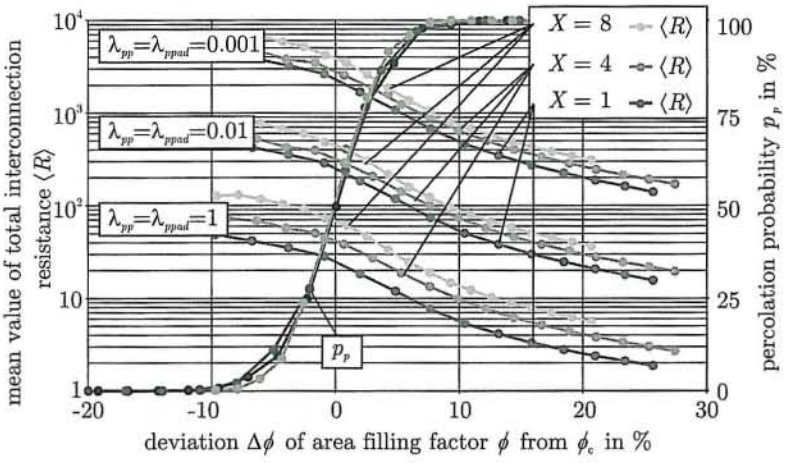

FIGURE 21.25. Results from Figure 21.24 but scaled as functions of the deviation $\Delta\phi$ of the filler content from the critical one for various cases of interfacial conductivity.

amount of filler content $\Delta\phi_{\min}$ which is needed in excess to ϕ_c to allow to form a reliably operating joint is the same in all three cases ($\Delta\phi_{\min} \approx 10\%$, Figure 21.25).

The practical meaning of this fact is that if the critical filler content of a system with a certain particle shape is known the necessary filler content of a system with a new particle shape can be found by increasing the filler content at least by the same percentage $\Delta\phi_{\min}$ as in the known system.

Having in mind the afore mentioned relation between the filler content and the mechanical qualities one would undoubtedly prefer adhesives with long particles, since the lower the filler content is the bigger are the expectable bonding forces. However, it turns out that the joint resistance at the same $\Delta\phi$ is also shifted to higher values in case of the longer particles: In the case of $X = 8$ the joint resistance is between two and three times as high as in case of $X = 1$. Since the electrical parameters of all simulations ($X = 1$, $X = 4$, and $X = 8$) remained unchanged the shift of joint resistance can only be explained by geometrical effects such as the size of overlapping areas characterizing the intensity of the contacts, the number B of neighboring particles which is responsible for the density of the resistance network, and the geometry of the particles themselves. However, it can be shown that B doesn't change significantly in all discussed cases. Thus, B is not responsible for the big resistance changes. If it is further determined that the size of the overlapping contact areas and therewith the respective widths $w_{s,i}$ of the particles are only slightly depending on the filler content one can realize that the main part of the joint resistance change has to be assigned directly to the particle shape.

Besides the results of the case $\lambda_{pp} = \lambda_{ppad} = 1$ the joint resistance functions of the cases $\lambda_{pp} = \lambda_{ppad} = 0.01$ and $\lambda_{pp} = \lambda_{ppad} = 0.001$ are also demonstrated in Figure 21.25. A constant vertical shift of corresponding curves indicates that in all cases an increase of the axis relation X causes an increment of $\langle R\rangle$ of almost the same amount. This applies also for the dependence of the joint resistance functions on the interparticle conductivity.

For practical applications it can be concluded from this model that the particle shape (in the model represented by the aspect ratio for elliptical particles) has a certain influence on the joint resistance. However, the influence of the same relative change of filler content is much stronger. Moreover it can be observed that the joint resistance has a weaker depen-

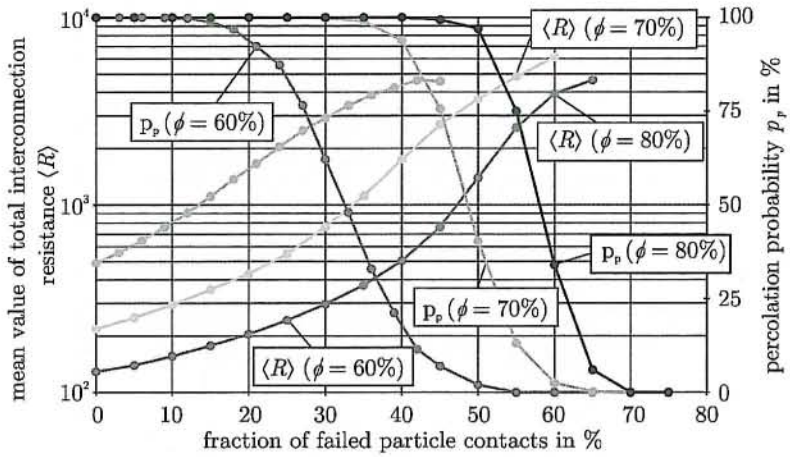

FIGURE 21.26. Joint resistance and percolation probability versus percentage κ_o of failed interparticle contacts for three values of filler content (particle parameters: $X = 4$, $A = 0.02^2 \cdot \pi$).

dency on the interparticle conductivity at high values of λ_{pp} and λ_{ppad} (a change of two orders of magnitude causes a resistance increase of only one order of magnitude). However, the more the interparticle conductivity decreases the more the joint resistance approaches to the inversely proportional dependence on the interparticle conductivity. Such a change could take effect if the molecular bonding forces of the polymer are weakened and oxides are formed at the particles interfaces.

As known from numerous investigations of the aging behavior under real operation conditions as well as under accelerated aging conditions the joint resistance can increase significantly [40–43]. By anticipating that changes do not occur in the volume of the conducting particles the resistance increase has to be assigned to degradation of the interfaces between particles and pad. The following part of the discussion is devoted to changes of the joint behavior due to aging.

In Figure 21.25 the shift of joint resistance with falling interparticle conductivity can be observed in cases when all interparticle contacts become homogeneously deteriorated to the same extent in the whole contact. However, this will remain the exception, since with growing thickness the contribution of tunneling becomes the dominant effect for the conductivity through the interface barriers. The initial specific tunneling conductivity e.g., on a noble metal surface is in the order of 10^{12} S/m^2 and with continuous growth of an oxide layer the conductivity decreases rapidly [44]. With respect to microscopic inhomogeneities in the ICA in a more realistic consideration, therefore, it should be assumed that due to e.g., oxidation more and more transitions between particles fail rather than that the interparticle conductivity decreases continuously and equally distributed. The results of simulations of such an aging behavior for joints with three different values of filler content ($\phi = 60\%$, $\phi = 70\%$, and $\phi = 80\%$) are demonstrated in Figure 21.26. For this purpose, the interparticle conductivity of a certain percentage of particle transitions are changed from $\lambda = 0.001$ to $\lambda = 0$ which means a total drop-out of the respective transitions. This percentage can be interpreted as the probability κ_o for such a drop-out. Thus, an increase of κ_o corresponds to an aging process in the ICA interconnection. At the beginning of the increase of κ_o only the joint resistance increases whereas the percolation probability remains constant at 100%. Only with continuing aging also the percolation probability starts to fall, indicating failing

of the joint to the respective percentage. It is obvious, that joints with a higher filler content have a lower joint resistance and will withstand a longer aging process without failing which could be interpreted some how as a better long-term reliability. However, it is remarkable that the joint resistance in the moment when the percolation probability starts falling below 100% is almost independent from the filler content.

The change of contact resistance for various types of ICAs, different curing processes, and aging conditions were also experimentally investigated [45] and are summarized in the following section.

21.3. AGING BEHAVIOR AND QUALITY ASSESSMENT

21.3.1. Introduction

Besides the benefits mentioned in the introduction, ICAs provide an environmentally friendly alternative to solders for interconnections in electronic applications with the advantage of a superior fine pitch capability. However, unstable electrical conductivity under elevated temperature and humidity conditions and a low impact resistance of the interconnections were major obstacles preventing ICAs from becoming a general replacement for solders in SMT until now.

It is a well accepted opinion that corrosion is involved in the shift of contact resistance [20,24,46,47]. It is reported that galvanic corrosion rather than simple oxidation is the dominant interfacial degradation mechanism. However, galvanic corrosion doesn't only need an electrochemical potential difference but would also require a ions-containing aqueous phase which would have to be formed at e.g., 85% r.h.—that means at a humidity level where wet surfaces usually dry-up. On the other hand, galvanic corrosion would be an explanation why a much faster increase in resistance is attained under elevated humidity than under dry conditions at the same elevated temperature [25].

Recently developed ICAs promise an improved electrical and mechanical reliability on non noble metalizations as conventionally used in SMT and can be completely cured in the same short duration as known from a typical reflow soldering cycle. In order to investigate connections between processing parameters and the aging behavior eight different ICAs for solder replacement from four mayor manufactures were evaluated with respect to the behavior of the contact resistance and the shear force during a forced aging process. For this purpose test assemblies with ICA sample contacts were fabricated using PCBs with the four most common surface finishes. The test assemblies were then exposed to an elevated temperature and humidity environment (85°C/85% r.h.) for 1000 h, whereby the changes of the electrical contact resistance and the shear force were monitored.

The test assemblies consisted of SMD-chip components (1206 and 0805) which were mounted on FR4-printed circuit boards with the sample contacts between different surface finishes and the respective component metalization. Two different curing methods were investigated: curing in a conventional convection oven and curing in a vapor phase device.

The goal of this study was to experience advantages and drawbacks of ICAs presently available on the market and to present some recent progresses in ICA technology development.

21.3.2. Material Selection and Experimental Parameters

All selected adhesives are one component, epoxy based, thermosetting, silver filled and isotropically conductive. All are especially designed to replace solder pastes in SMT.

According to the manufactures data sheets, some of them promise a stable contact resistance even when applied on tin, tin/lead and OSP-coated copper. Table 21.1 gives an overview about the selected products and curing conditions as recommended by their manufacturers.

The test boards were pluggable and allowed to combine monitoring of contact resistance shift with the four-point probe method of 40 contacts simultaneously during forced aging (Figure 21.27), and after that mechanical quality testing.

In this way the voltage drop of the series connection of two joint resistances and the resistance of the component itself is measured. In order to keep uncertainties during evaluation of the joint resistance as small as possible chip resistors (1206 and 0805 package) with a low value and a small tolerance (51 mΩ ±5%) were used provided with lead free galvanic tin coated contacts. The joint resistance is defined as the resistance between contact pad and metalization of the component. The voltage drop within the copper pads and the metalization of the component can be neglected in this arrangement.

TABLE 21.1.
Chosen ICAs with the curing conditions as recommended by the manufactures.

Manufacturer	Adhesive	Recommended curing conditions
A	1	120 min @ 120°C
		30 min @ 140°C
	2	5 min @ 125°C-Reflow
		3 min @ 150°C-Reflow
		8 min @ 125°C-Convection
		5 min @ 150°C-Convection
B	1	30 min @ 125°C
		15 min @ 150°C
	2	120 min @ 125°C
		60 min @ 150°C
C	1	10 min @ 125°C
		6 min @ 150°C
		3 min @ 175°C
	2	6 min @ 130°C
		3 min @ 150°C
D	1	30 min @ 140°C
	2	N.A.

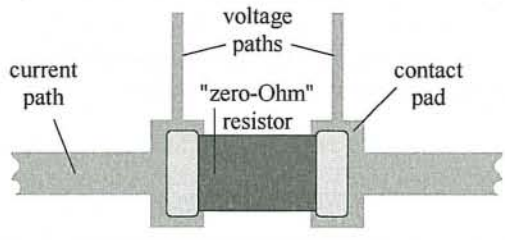

FIGURE 21.27. Conductor structure of one component.

With respect to the most commonly used surface finishes of PCBs test boards with the following types of surface treatments were manufactured:

- organic surface protection (OSP): ENTEK Plus Cu-106A
- electroless Ag-coating
- electroless Ni/Au-coating
- electroless Sn-coating.

The curing cycles were optimized by monitoring the electrical conductivity of the bondings during the curing process. This method is explained in the following subsection.

21.3.3. Curing Parameters and Definition of Curing Time

The results of quality testing of ICA joints depend strongly on how the adhesive has been cured. A comparison of quality, therefore, needs a thorough definition of curing conditions. Two different curing methods were applied in comparison. The first one as reference was curing in a conventional convection oven at a preselected temperature (two values were considered: 150°C or 200°C). The second method was curing in a saturated vapor phase of perfluorinated fluids with boiling points of 155°C and 200°C. The idea of using vapor phase condensation is to take advantage of the much higher heat transfer rates compared to gas convection allowing to shorten down the relatively long curing time of most ICAs to the length of a typical reflow soldering cycle by reducing the heating-up time.

In general ICAs have a high electrical resistance before curing. The conductivity develops during the curing process [48]. It is assumed that shrinkage of the resin matrix during curing causes the silver flakes to contact more intimately which leads to the dramatic contact resistance decreases [49]. If the relation between conductivity and curing degree of the adhesive is known for the respective combination of adhesive and curing method it can be used to determine the needed curing time. Figure 21.28 shows how the conductivity develops during the curing process. For this purpose, calibration measurements were performed with samples where the adhesive was printed over a spacing between two contact pads forming a quadratic resistor (length and width: 1 mm, thickness: 100 μm). The resistance between these contact pads was observed during the curing process. Reliable representa-

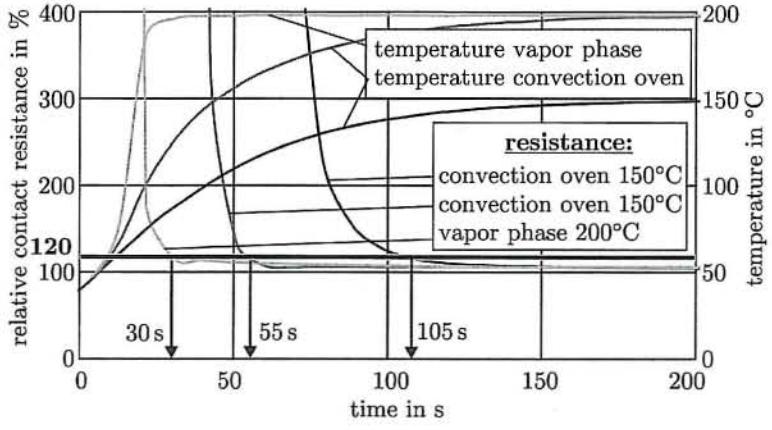

FIGURE 21.28. Change of contact resistance during curing process (adhesive type A1).

TABLE 21.2.
Applied curing times in minutes required to achieve 120% of the minimum possible resistivity.

Adhesive	Convection		Vapor phase	
	150°C	200°C	155°C	200°C
A1	8	3	2	2
A2	8	4	5	3
B1	20	4	15	3
B2	40	20	30	10
C1	8	2	3	2
C2	8	2	3	2
D1	8	5	6	3
D2	8	5	6	3

tive calibration curves were obtained by averaging results from six measurements at each combination. This kind of contact resistance measurement is an easy and reliable method of online monitoring of the curing progress allowing to closed-loop control the curing time and to optimize the curing condition for PCBs with different thermal properties.

Figure 21.28 shows the result of these measurements for curing the A1-type adhesive at 150°C and 200°C in the convection oven and for curing at 200°C in the vapor phase device. Curing at 200°C in the convection oven causes a faster decrease of the resistance as at 150°C due to the faster polymerization process. However, the resistance drop at curing the adhesive with 200°C in the vapor phase device is still much earlier and faster due to the significantly reduced heating-up time of the sample. As an indicator for the completion of the curing process the moment is used when the average resistance reaches the 120% mark of its final value (which was obtained from reference samples after a curing time of 1 hour). The time span until this moment multiplied by a safety factor was rounded up to at least 2 min. This time was defined as curing time for each evaluated adhesive/curing method combination and used for the further sample preparation. Table 21.2 gives a summary of the curing times determined in this way. In general the curing time as defined above is shorter than the one recommended in Table 21.1.

21.3.4. Testing Conditions, Typical Results, and Conclusions

For each particular combination of material and curing method the testing results from 80 adhesive joints were established. To evaluate the reliability of the contacts these samples were exposed to an elevated temperature and humidity (85°C/85% r.h.) environment for 1000 hours. During this forced aging process the electrical contact resistance was measured every 100 hours at room temperature and the results were averaged. The shear force was measured in the initial state, after 400, and after 1000 hours. At every measurement 6 to 7 components were sheared off. If either the contact resistance was higher than 5 Ω or the component dropped off from the test board the contact was counted as "failed" and not considered in further evaluations.

21.3.4.1. Influence of PCB finish on aging behavior The A1 type is a commercially applied ICA but not especially designed for the use on less noble metal surfaces. Therefore, it is not surprising that joints fabricated with this adhesive show a drastic increase of contact resistance during the testing period on PCB finishes like tin or copper [50,51]. Since the

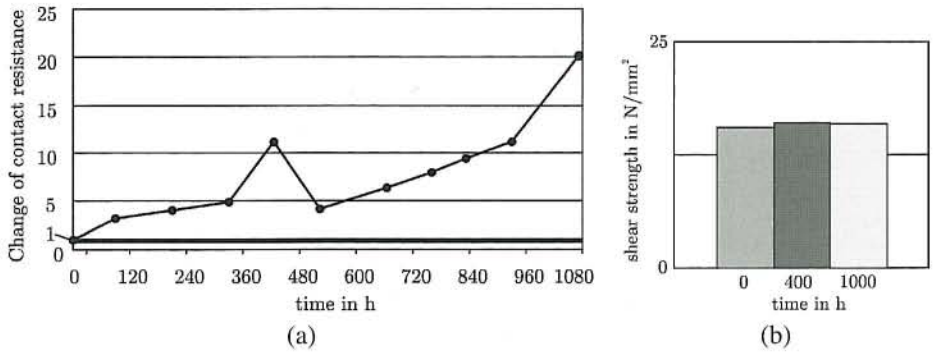

FIGURE 21.29. Adhesive A1 on Ag-coated PCB during forced aging test (85°C/85% r.h.); curing at 150°C in the convection oven. (a) Change of joint resistance (initial value: 10 mΩ). (b) Change of shear force.

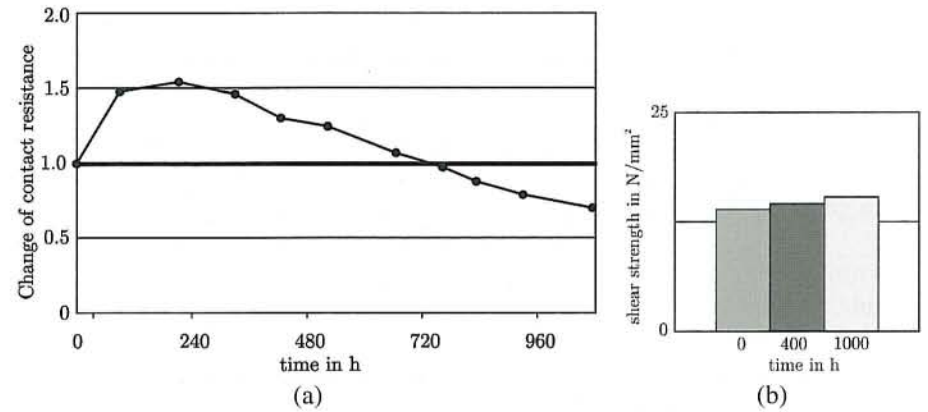

FIGURE 21.30. Adhesive A1 on Sn-coated PCB during forced aging test (85°C/85% r.h.); curing at 150°C in the convection oven. (a) Change of joint resistance (initial value: 37 mΩ). (b) Change of shear force.

increase of contact resistance is observable on each of the tested PCB-finishes it is assumed that the interface between the ignoble tin surface of the component and the adhesive is responsible for this effect. Despite of the high shift of contact resistance the shear strength did not decrease. Figure 21.29 shows the results measured at the Ag-coated PCB cured in the convection oven at 150°C.

The more recently developed product A2 is designed for solder replacement and suitable also for mounting components with tin surfaces. On all samples the average contact resistance after the forced aging test was even lower than the initial value. For the samples cured in the convection oven at 150°C only a slight increase of contact resistance in the first quarter of the testing time and a subsequent decrease of the resistance were observed. Figure 21.30 shows the results obtained from Sn-coated PCBs cured in the convection oven at 150°C. Also the shear force shows stable values over the entire testing period. Only at the NiAu coated PCB a decrease of the shear force was noticeable.

Another example is a product C2 offered as a comparatively quickly curing adhesive (3 minutes at 200°C) showing a strong increase of resistance only on the Sn-coated PCB. Rather high initial values decreased significantly after about 300 hours of aging (Figure 21.31). The used curing time of only 2 minutes was certainly insufficient.

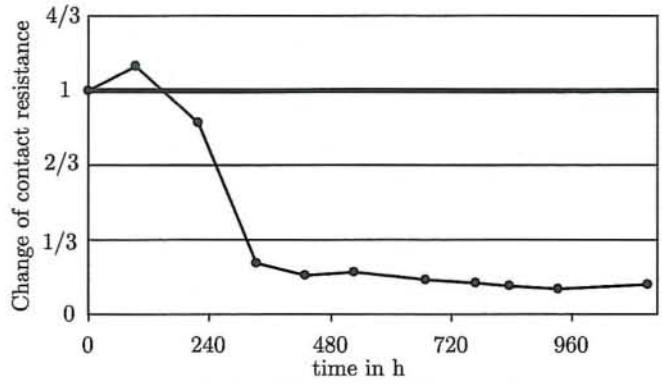

FIGURE 21.31. Change of contact resistance; adhesive C2 on OSP-coated PCB during forced aging test (85°C/85% r.h.); cured at 200°C in the convection oven.

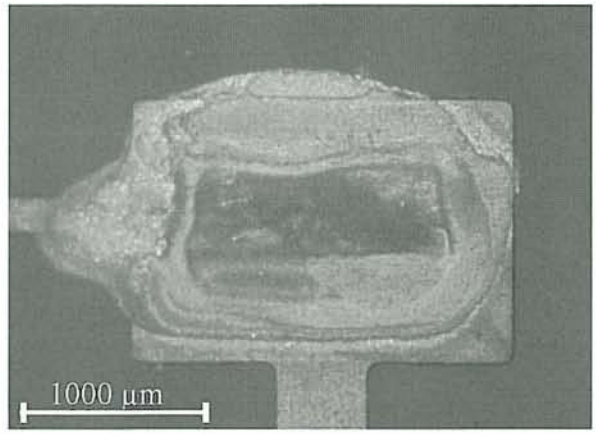

FIGURE 21.32. Area of fracture after shear test after 1000 hours forced aging (adhesive D2, curing condition: vapor phase 155°C, PCB OSP-coated).

Figure 21.32 depicts an area of fracture after a shear test of a sample joint manufactured with adhesive D2 after 1000 hours of aging. The fracture occurred at the PCB/adhesive–interface. A discoloration of the pad surface is visible resulting from a strong degradation of this interface. It should be noted that a low shear force can appear independent from a good conductivity.

By contrast, Figure 21.33 shows the area of fracture of a contact formed with adhesive D1 using the same parameters as in Figure 21.32. In this case the fracture occurred mainly at the component/adhesive interface. At the PCB pad where the fracture occurred a blank, shiny copper surface appeared indicating a low degradation. It is not surprising that this sample showed good mechanical and electrical properties.

21.3.4.2. Summary Eight different ICAs from four mayor manufactures were evaluated with respect to there suitability to serve as replacement of solder pastes. As a general result it should be noted that significantly different behavior of the tested adhesives could be observed in spite of consisting of quite similar compositions: silver-filled one-component epoxy resin.

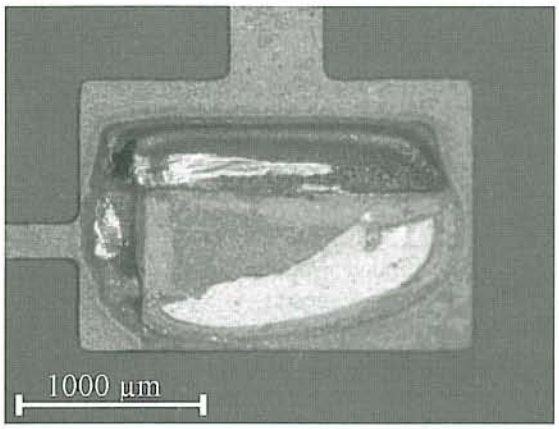

FIGURE 21.33. Area of fracture after shear testing a sample with a type D1 adhesive after 1000 hours forced aging (curing condition: in vapor phase at 155°C, PCB: OSP-coated).

Adhesives of the A1-type and D1-type are not recommended for oxygen rich systems or oxidizing surfaces from their manufacturers. Although, initial values of joint resistivity and shear strength were acceptable, the results during and after a forced aging process exhibit large shifts and an unstable values.

Using the vapor phase device generally the curing time of the adhesives can be decreased drastically due to the high heat transfer rate obtained by condensation. Although, with some adhesives perfect results were obtained with others the shear strength showed significantly lower values compared to equal samples cured in the convection oven. Further investigations would be required to fully understand the reasons for these different behaviors.

Using the NiAu-finished PCBs an increased failure rate was observable for the most adhesives. At the first glance this might be surprising since due to the low inclination to oxidation of noble metal surfaces one could expect a rather moderate tendency to changes of the contact resistance. However, the increase of resistance during aging might to a certain extent be assigned to the weaker adhesion between gold and the epoxy resin. The latter argument is in good agreement with the results of the shear tests frequently showing the area of fracture coinciding with the gold-adhesive interface.

The newer ICA types didn't show a significant increase of contact resistance during a forced aging under elevated temperature and humidity even on ignoble metal surfaces as well as on the OSP coated copper pads. Although, the protective layer could be assumed to impede an intimate contact between the filler particles and the metalization, rather the opposite turns out from the investigations as described afore. No retardation of the onset of contact formation during curing can be observed and a stable joint resistance during aging can be understood as an indicator for a reliable long-term behavior.

As a summarizing result of this investigation it can be concluded that the progress of the adhesive technology has reached a stage were a replacement of solder by an isotropic conductive adhesive can be performed in many cases without changing the involved surfaces treatments whereby a reliability level can be achieved comparable to solder joints.

21.4. ABOUT TYPICAL APPLICATIONS

Due to the large variety of filler content and chemical composition of the polymer the industrial use of ICAs is not restricted to the attachment of SMDs. The following examples demonstrate the numerous application fields.

21.4.1. ICA for Attachment of Power Devices

For optimizing device performance and reliability of power devices an accurate thermal design is a critical issue. The basic need is to remove the power loss produced in the device (junction) under operation condition at the lowest possible temperature drop with respect to the ambient. This quality is expressed as the junction-to-ambient thermal resistance $R_{th,j-a}$. It consists of the sum of the junction-to-case thermal resistance $R_{th,j-c}$ and the thermal resistance $R_{th,c-a}$ from the case to the ambient. Whereas $R_{th,j-c}$ is provided in the datasheet from the component's manufacturer $R_{th,c-a}$ highly depends on the mounting technique and can vary orders of magnitude. In power assemblies the device case is attached to a heat sink using a thermal grease, by adhesive bonding, or by soldering. Normally, heat dissipation from the case by radiation and convection can be neglected. $R_{th,c-a}$ is mainly controlled by the heat flow through the bond line between the device case and the heat sink. Therefore, $R_{th,j-a}$ can be expressed as

$$R_{th,j-a} = R_{th,j-c} + R_{th,c-a} = R_{th,j-c} + R_{th,bond} + R_{th,heatsink}, \tag{21.7}$$

where $R_{th,heatsink}$ is defined as the thermal resistance between the mounting surface of the heat sink and the ambient. The bond line thermal resistance $R_{th,bond}$ can in principle be calculated by dividing the expected or measured bond line thickness by the adhesive's intrinsic thermal conductivity λ_{bond} measured on a free-standing cured sample. However, at a typical bond line thickness of 15–75 μm, the interface thermal resistance $R_{th,if}$ between the adhesive and its adherents can be significant compared to the intrinsic thermal resistance of the adhesive and thus the bond line thermal resistance itself must be considered as a sum of the two components [52]

$$R_{th,bond} = \frac{t_{bond}}{A \cdot \lambda_{bond}} + R_{th,if}, \tag{21.8}$$

where A and t_{bond} are the bond line area and thickness. The practical importance can be seen on the example of a TO-247 package which is attached to a heat sink with a copper heat spreader as mounting surface (Figure 21.34). Two types of ICAs are compared: a conventional one with a low thermal conductivity and an ICA (type Diemat DM6030Hk) with a silver particle content of more than 95 weight percent.

For mounting the device on a heat sink, the ICA must flow as freely as grease to eliminate air voids and reduce the thermal resistance of the interface. However, a complete avoidance of pores and gas enclosures in the bond line is not always possible. In order to consider the thermal meaning of enclosures in the bond line Equation (21.8) has to be modified such that the thermally conducting cross section of the ICA is reduced by the area percentage p of the voids:

$$R_{th,bond} = \frac{1}{A} \cdot \frac{t_{bond}}{\lambda_{bond} \cdot \left(1 - \frac{p}{100}\right) + \lambda_{air} \cdot \frac{p}{100}} + R_{th,if}. \tag{21.9}$$

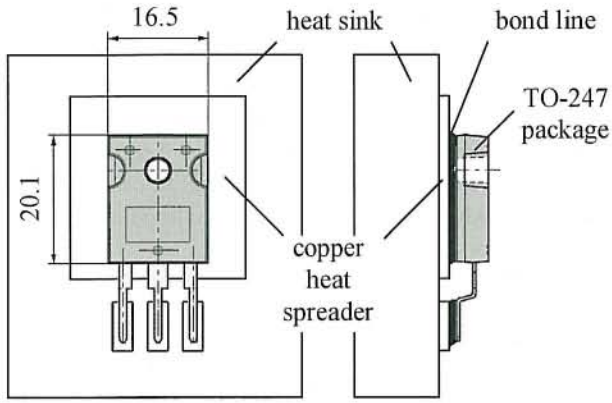

FIGURE 21.34. Power device assembly with TO-247 package (dimensions in millimeter).

TABLE 21.3.
Geometry and thermal data used for evaluation as demonstrated in Figure 21.35.

Bond line thickness	in μm	50	
Bonding area	in cm^2	2.31	
Thermal conductivity of voids (air)	in W/(m°C)	0,03	
Thermal conductivity of conventional ICA	in W/(m°C)	2	[53]
Thermal conductivity of DIEMAT ICA	in W/(m°C)	60	[53]
Thermal conductivity of Sn96Ag3.5Cu	in W/(m°C)	57	[54]
$R_{th,if}$ at bonding area of 2.31 cm^2	in °C/W	8.7×10^{-2}	[52]

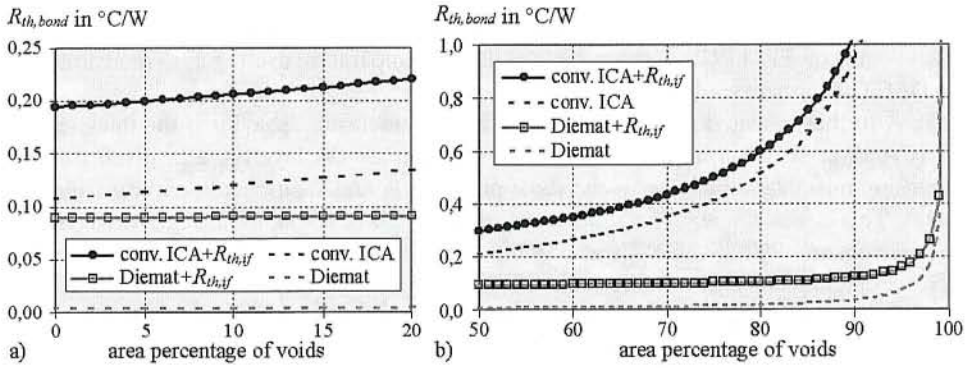

FIGURE 21.35. Bond line thermal resistance $R_{th,bond}$ versus percentage of gas enclosures; (a) at acceptable quantities of enclosure, (b) in an unacceptable range.

Using the values as listed in Table 21.3 Equation (21.9) is evaluated for different ICA types.

At low percentages of enclosures an almost linear increase of $R_{th,bond}$ can be observed in bond lines with conventional ICAs. No measurable thermal effect of enclosures exists in case of a high intrinsic thermal conductivity (DIEMAT or lead-free solder). In order to recognize the meaning of the interface thermal resistance for both ICA types $R_{th,bond}$

is also calculated as a reference with $R_{th,if}$ set to zero (dashed curves), respectively. In both cases the interface thermal resistance clearly predominates the thermal resistance increase due to enclosures [Figure 21.35(a)]. It is surprising that only if voids are unacceptably large from mechanical point of view they become thermally important [Figure 21.35(b)].

For $R_{th,j-c}$ of silicon devices in TO-247 packages frequently values below 1°C/W are provided from manufacturers. It should be noted that in cases of GaAs power devices due to the lower thermal conductivity of the substrate compared to Si the discussed phenomena are particularly important [53].

21.4.2. ICA for Interconnecting Parts with Dissimilar Thermal Expansion Coefficient

For many types of radiation sensors sealed housings are needed consisting of a metal cap and a base plate which carries the sensor substrate. The base plate including the bonding process for mounting the sensor substrate is dispensable if all functions of the base plate can be fulfilled by the sensor substrate itself. The cap can either be soldered to the substrate using a high-temperature solder in order to allow a second soldering process (e.g., for its attachment to a PCB) or an adhesive can be applied. The latter is favored whenever a low processing temperature is essential or when thermomechanical requirements cannot be fulfilled with a soldered joint. In the following example an alumina substrate with a wiring structure produced by thick film technology was required to be bonded to a cap of aluminum whereby soft soldering had to be excluded from the possible joining techniques, since due to very dissimilar coefficients of thermal expansion of base plate and cap thermal cycling caused microcracks in the solder layer. The basic structure of the sensor is schematically illustrated in Figure 21.36.

Adhesives with a high glass transition temperature T_g are reported as to be generally more susceptible to the formation of cracks than those with a low T_g which is understood as a different ability to stress relaxation [55]. However, due to the thermoelastic behavior of adhesives there are e.g., the possibility of directly attaching of 15 mm × 15 mm large silicon chips on FR-4 PCB without damage during temperature cycling as demonstrated in the DACTEL project [56].

A further essential parameter besides the thermoelastic behavior is the thickness of the ICA layer between the mating surfaces. The thicker the layer is, at a given thermal expansion mismatch, the lower is the shear plane angle and the inclination to formation of cracks. This is well known from reliability investigations of solder joints e.g., between chip components and PCBs where it was found that the number of thermal cycles until failure increases significantly with rising stand-off height [57].

Besides aspects of long-term reliability the housing of the sensor has to fulfill thermal requirements. An accurate calibration of the sensor frequently needs a constant temperature distribution in the housing. Therefore, the heat loss has to be dissipated from the substrate through a clamping part at the front face of the cap at the lowest possible temperature drop. From this consideration a thin bonding layer is needed which is in contradiction with the mechanical requirements. An optimum can be found by selecting an adhesive with a high thermal conductivity. Figure 21.37 depicts the result of a comparison of two axial temperature profiles in the cap obtained by thermal simulation. This study shows that the temperature drop perpendicular to an ICA layer can be reduced significantly by increasing the filler content. Whereas the thermal conductivity of adhesives for conventional surface mounting applications even if offered as thermally conductive adhesives is rather low (ranging in the order of some W/mK, [58], represented by type 1 ICA in Figure 21.37) there are some

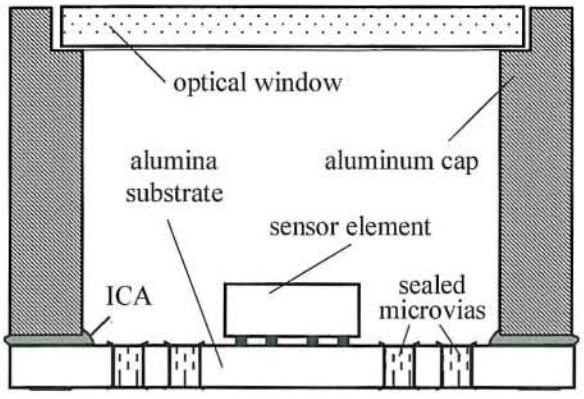

FIGURE 21.36. Schematic structure of the sensor housing.

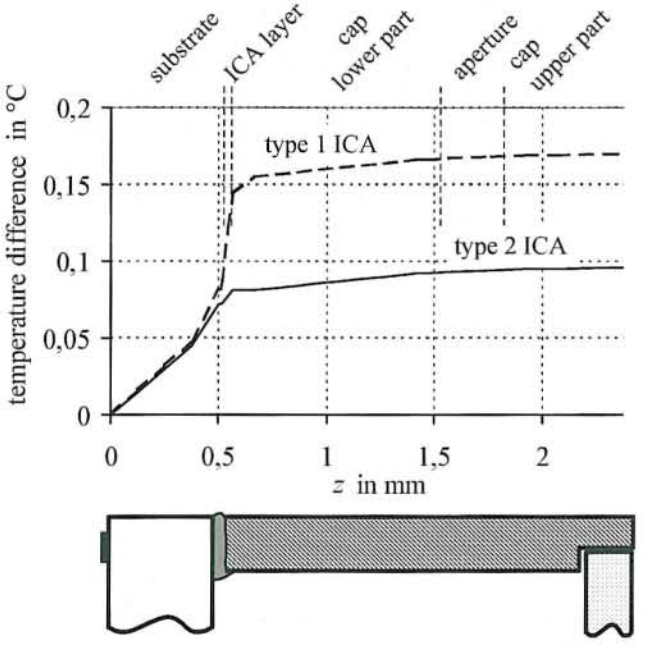

FIGURE 21.37. Influence of the thermal conductivity of the ICA layer on the temperature profile in axial direction (type 1 ICA: 3 W/mK, type 2 ICA: 30 W/mK).

types of ICA on the market with an extremely high silver content with a thermal conductivity of more than 50 W/mK (type 2 ICA, filler content: 93 weight % silver, 60 W/mK), allowing to achieve a negligible temperature drop across the ICA layer.

Due to the excellent thermoelastic behavior of the adhesive a lateral displacement of up to 20 μm due to different thermal expansions of substrate and cap could be handled with an adhesive layer thickness of only about 30 μm [59].

TABLE 21.4.
Comparison of number of process steps for SMD assembling either using soldering (left column) or adhesive bonding (right column).

...	...
Printing the solder (stencil) for SMDs and the transistor chip	Printing the adhesive (stencil) for all components
Placing SMDs and transistor	Placing all components
Reflow soldering	Curing the adhesive
Cleaning (flux removing)	–
Dispensing the adhesive for the remaining chips	–
Placing the chips	–
Curing	–
Wire bonding	Wire bonding
Applying glob top	Applying glob top
...	...

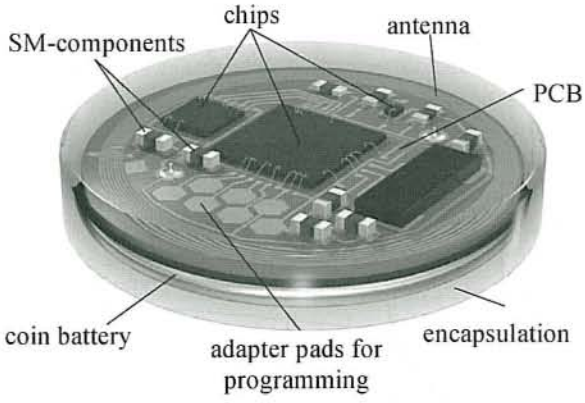

FIGURE 21.38. Schematic illustration of the temperature logger module.

21.4.3. ICA for Cost-Effective Assembling of Multichip Modules

Frequently multichip modules are the solution when a high degree of miniaturization is needed in an electronic assembly with complex functions. The application described here is a temperature logger system smaller than a one-Euro cent coin in diameter embedded in a removable brace to observe the wearing habits of the patient [60]. For this purpose the temperature is measured with a pn junction and recorded using a microcontroller which acts as a temperature logger and is capable of storing the thermal history from several months. This device is hermetically sealed using polymeric encapsulants. A wireless data exchange is performed using a radio frequency identification device (RFID). The electronic assembly contains a printed circuit board which is populated with SMDs in 0201 package (0.6 mm × 0.3 mm) and bare microprocessor and RFID chips (Figure 21.38).

The SMDs can be assembled by soldering or ICA bonding. The die components were not available for solder attachment as is frequently the case for small-batch production. Thus, wire bonding was necessary in the vicinity of the SMDs. In order to prevent the wire bonding pads from flux residues, the attachment of the SMDs by soldering would be related to additional process steps for protection and for cleaning of the bonding pads. The production process with the lowest possible number of process steps was found using ICA

for the attachment of chips and SMDs [59]. The manufacturing processes are compared in Table 21.4.

21.5. SUMMARY

As a historical background the development of ICA technology is briefly discussed. Already decades ago some principle advantages were recognized such as the low processing temperature and the possibility to use non-wettable and base metal surfaces for interconnections. For this reason, the attachment of semiconductors was the first application of ICAs in electronic packaging. In the meanwhile, much progress has been achieved in the quality and stability of ICA materials. Nevertheless, the ICA technology is not widely seen as an equivalent replacement of soldering, although it is a lead-free and a flux-free technology and both of these facts are important environmental aspects. One reason might be the experience with the former ICA technology concerning a moderate long-term reliability due to the inclination of oxide formation and galvanic corrosion in humid environment at elevated temperature. One goal of this contribution is to provide a deeper understanding of silver filled epoxy-based adhesives. For this purpose a model of an ICA joint which considers the particle alignment and distribution as well as the voltage and current distribution within the adhesive is discussed. Using this model the influence of parameters like filler content, particle arrangement, and particle size on the joint resistance is estimated and tendencies of changes during aging are clarified. The behavior of real ICA joints under accelerated aging condition and the results of quality assessment is also discussed. Finally, some practical examples demonstrate advantages and drawbacks in manifold fields of applications.

NOTATIONS AND DEFINITIONS

A	particle area
A_{ex}	excluded area
$\langle A_{ex} \rangle$	mean value of excluded area
A_{ex}/A	normalized excluded area
B	mean number of neighbored particles
B_c	mean critical number of neighbored particles
δ	angle between major axes of two particles
ϕ	portion of area filled with particles (filler content in area %)
ϕ_c	critical portion of area filled with particles (critical area filling factor)
$\Delta\phi$	deviation of area filling factor ϕ from critical value ϕ_c
γ	angle between major axes of a particles and the (horizontal) pad plane
κ_o	probability for a nonconductive (failing) interconnection between two particles
λ_{pp}	specific interface conductivity between two particles, see Equation (21.1).
$\lambda_{p\,pad}$	specific interface conductivity between particle and pads
p_c	percolation probability of 50%
p_p	percolation probability
R	normalized total resistance of interconnection (joint resistance)
$\langle R \rangle$	mean value of the normalized total interconnection resistance
R_{pp}	transition resistance between two particles

$R_{p\,pad}$	transition resistance between a particle and a pad
$\langle R_{tr} \rangle$	total transition resistance at both pad-particle interfaces, average value
σ	specific conductivity of particle
σ_{pad}	specific conductivity of pad
w_{tot}	total width of the modeled space (= length of the contact pad)
$w_{s,i}$	contact width at the ith particle (length of intersection line between two considered particles or between particle and the pad as e.g., shown in Figure 21.3)
$w_s^* = \sum_i^n w_{s,i}$	total effective width of contact pad (= active width of pad involved in current flow), n is the number of particles in direct contact with the respective pad and contributing to current flow
$\langle w_s^*/w_{tot} \rangle$	percentage of total effective contact width with respect to the pad length, average value
X	length relation between major and minor axis of elliptical particles (axis relation)

REFERENCES

1. R.L. Henry, Improvements in commutator brushes, British Patent #246.972, 1926.
2. H. Schuhmann, Conductive varnish, U.S. Patent #1,913,214, June 6, 1933.
3. H. Bienfait and W.L. Carolus van Zwet, Electrical conductor and method of making the same, U.S. Patent #2,018,343, Oct. 22, 1935.
4. H.J. Loftis, Molded electrically conductive body, U.S. Patent #2,361,220, Oct. 24, 1944.
5. N.H. Collings and R.J. Heaphy Beverton, Electrically conductive adhesive, U.S. Patent #2,444,034, June 29, 1948.
6. H. Wolfson and G. Elliott, Electrically conducting cements containing epoxy resins and silver, U.S. Patent #2,774,747, Dec. 18, 1956.
7. C. Mitchel and H. Berg, Use of conductive epoxies for die-attach, Int. Symp. Microelectron, 1976.
8. D. Gerber and W. Scheel, Kleben elektronischer Baugruppen, in W. Scheel, Ed., Baugruppentechnologie der Elektronik, Verlag Technik Berlin, Eugen G. Leuze Verlag, Saulgau, 1997, pp. 393–394.
9. H. Shirakawa, Nobel lecture: The discovery of polyacetylene film—the dawning of an era of conducting polymers, Reviews of Modern Physics, 73(July), pp. 713–718 (2001).
10. P.M. Raj, J. Liu, and P. Öhlckers, Fundamentals of packaging materials and processes, in R.R. Tummala, Ed., Microsystems Packaging, McGraw-Hill, 2001, p. 739.
11. I. Watanabe and K. Takemura, Anisotropic conductive adhesive films for flip-chip interconnection, in J. Liu, Ed., Conductive Adhesives for Electronics Packaging, Electrochemical Publications Ltd., ISBN 0 901150 37 1, 1999, pp. 256–271.
12. A. Aghzout, Über die Leitfähigkeit von elektrisch anisotropen Klebern und deren Anwendungen in der Mikroelektronik, Dissertation thesis, Vienna University of Technology, June, 2002.
13. K.-i. Shinotani, J. Malmodin, and R. Trankell, Fundamentals of microsystems design for environment, in R.R. Tummala, Ed., Microsystems Packaging, McGraw-Hill, 2001, p. 859.
14. G. Hanreich, K.-J. Wolter, and J. Nicolics, Rework of flip-chip polpulated PCBS by laser desoldering, in H. Hauser, Ed., Sensors & Packaging, ÖVE-Schriftenreihe, Nr. 35, 2003, pp. 283–289.
15. L.M. Yu and W.C. Qing, Solder joints design attribute to no solder bridge for fine pitch device, Fifth International Conference on Electronic Packaging Technology, ICEPT2003, Shanghai, China, 28–30 Oct., 2003, pp. 70–75.
16. S. Kang, R.S. Rai, and S. Purushothaman, Development of high conductivity lead (Pb)-free conductive adhesives, IEEE Transactions on Components Packaging, and Manufacturing Technologies, 21(4), pp. 18–22 (1998).
17. J.S. Hwang, Fine pitch soldering and solder paste, in J.H. Lau, Ed., Handbook of Fine Pitch Surface Mount Technology, Van Nostrand Reinhold, New York, 1993, pp. 81–133.
18. Directive 2002/95/EC of the European Parliament and of the Council of 27 January 2003 on the Restriction of the Use of Certain Hazardous Substances in Electrical and Electronic Equipment, Official Journal of the European Union L37, 13.02.2003, pp. 19–23.

19. R. Dudek, H. Berek, T. Fritsch, and B. Michel, Reliability investigations on conductive adhesive joints with emphasis on the mechanics of the conduction mechanism, IEEE Transactions on Components and Packaging Technologies, 3(3), pp. 462–469 (2000).
20. C.P. Wong and D. Lu, Recent advances in electrically conductive adhesives for electronics applications, 4th International Conf. on Adhesive Joining and Coating Technology in Electronics Manufacturing, Proceedings, 2000, pp. 121–128.
21. S. Ganesan and M. Pecht, Lead-free electronics—2004 Edition, CALCE EPSC Press, ISBN 0-9707174-7-4, 2004.
22. J.H. Lau, C.P. Wong, N.-C. Lee, and R.S.W. Lee, Electronics Manufacturing—with Lead-Free, Halogen-Free, and Conductive-Adhesive Materials, McGraw-Hill, ISBN 0071386246, July 2002.
23. J.E. Morris, F. Anderssohn, S. Kudtarkar, and E. Loos, Reliability studies of an isotropic electrically conductive adhesive, 1st Int. IEEE Conference on Polymers and Adhesives in Microelectronics and Photonics, October 21–24, Potsdam, Germany, 2001, pp. 61–69.
24. D. Lu and C.P. Wong, Development of conductive adhesives for solder replacement, IEEE Transactions on Components and Packaging Technologies, 23(4), pp. 620–626 (2000).
25. D. Lu, C.P. Wong, and Q.K. Tong, Mechanisms underlying the unstable joint resistance of conductive adhesives, IEEE Transactions on Components, Packaging, and Manufacturing Technology, Part C, 22(3), pp. 228–232 (1999).
26. M. Zwolinski, J. Hickman, H. Rubin, Y. Zaks, S. McCarthy, T. Hanlon, P. Arrowsmith, A. Chaudhuri, R. Hermansen, S. Lau, and D. Napp, Electrically conductive adhesives for surface mount solder replacement, IEEE Transactions on Components, Packaging, and Manufacturing Technology, Part C, 19(4), pp. 251–256 (1996).
27. E. Stanley, J.S. Andrade, S. Havlin, H.A. Makse, and B. Suki, Percolation Phenomena: a broad-brush introduction with some recent applications to porous media, liquid water, and city growth, Physica A: Statistical and Theoretical Physics, 266(1-4), pp. 5–16 (1999).
28. A. Bunde, Percolation in composites, Journal of Electroceramics, 5(2), pp. 81–92 (2000).
29. J.E. Morris, Conduction mechanisms and microstructure development in isotropic, electrically conductive adhesives, in J. Liu, Ed., Conductive Adhesives for Electronics Packaging, Electrochemical Publications Ltd., ISBN 0 901150 37 1, 1999, pp. 37–77.
30. M. Mündlein, J. Nicolics, and G. Hanreich, Accelerated curing of isotropically conductive adhesivemns by vapor phase heating, Third International IEEE Conference on Polymers and Adhesives in Microelectronics and Photonics (Polytronic 2003), Montreaux, Switzerland, October 21–23, 2003, pp. 101–105.
31. L. Li and J.E. Morris, Electrical conduction models for isotropically conductive adhesive joints, IEEE Transactions on Components, Packaging, and Manufacturing Technology, Part A, 20(1), pp. 3–8 (1997).
32. X.-G. Liang and X. Ji, Thermal conductance of randomly oriented composites of thin layers, International Journal of Heat and Mass Transfer, 43, pp. 3633–3640 (2000).
33. E. Sancaktar and B. Lan, Modeling filler volume fraction and film thickness effects on conductive adhesive resistivity, 4th IEEE International Conference on Polymers and Adhesives in Microelectronics and Photonics (Polytronic 2004), Portland, USA, 12–15 Sept., 2004, pp. 38–49.
34. I. Balberg, C.H. Anderson, S.Alexander, and N. Wagner, Excluded volume and its relation to the onset of percolation, Physical Review B, 30(7), pp. 3933–3943 (1984).
35. P.A. Cundall, A computer model for simulating progressive, large-scale movements in blocky rock systems, Proc. Symp. Int. Rock Mech. 2(8), Nancy, Vol. 2, 1971, pp. 129–136.
36. B. Su and J. Qu, A micromechanics model for electrical conduction in isotropically conductive adhesives during curing, Electronic Components and Technology 2004, Volume 2, 1–4 June 2004, pp. 1766–1771.
37. G.G.W. Mustoe, M. Nakagawa, X. Lin, and N. Iwamoto, Simulation of particle compaction for conductive adhesives using discrete element modeling, Electronic Components and Technology Conference 1999, 1–4 June, 1999, pp. 353–359.
38. A. Drory, I. Balberg, and B. Berkowitz, Application of the central-particle-potential approximation for percolation in interacting systems, Physical Review E, 52, pp. 4482–4494 (1995).
39. B. Berkowitz, Percolation theory and network modeling applications in soil, Physics: Surveys in Geophysics, 19(1), pp. 23–72 (1998).
40. S. Xu, D.A. Dillard, and J.G. Dillard, Environmental aging effects on the durability of electrically conductive adhesive joints, International Journal of Adhesion and Adhesives, 23(3), pp. 235–250 (2003).
41. E. Suganuma and M. Yamashita, High temperature degradation mechanism of conductive adhesive/Sn alloy interface, International Symposium on Advanced Packaging Materials: Processes, Properties and Interfaces, Proceedings, 2001, March 11–14, 2001, pp. 19–22.

42. H. Li, K.-S. Moon, Y. Li, L. Fan, J. Xu, and C.P. Wong, Reliability enhancement of electrically conductive adhesives in thermal shock environment, Electronic Components and Technology, ECTC 2004, Vol. 1, June 1–4, Las Vegas, USA, 2004, pp. 165–169.
43. F. Kriebel, Leitkleben—eine Alternative zum Löten in der Oberflächenmontagetechnik, VTE, (4)(Aug.), pp. 182–191 (1998).
44. H. Hauser, Kontaktwerkstoffe, Anhang D, in G. Fasching, Ed., Werkstoffe für die Elektrotechnik, Springer, 4th edition, 2005, pp. 517–520.
45. M. Mündlein, J. Nicolics, and J.E. Morris, Reliability investigations of isotropic conductive adhesives, 25th International Spring Seminar on Electronics Technology, ISSE 2002, Prague, Czech Republic, May 11–14, ISBN 0-7803-9824-6, 2002, pp. 329–333.
46. K. Gilleo, Evaluating polymer solders for lead-free assembly part I, Circuits Assembly, (January), pp. 50–56 (1994).
47. J.C. Jagt, P.J.M. Beris, and G.F.C.M. Lijten, Electrically conductive adhesives: a prospective alternative for SMD soldering? IEEE Transactions on Components, Packaging, and Manufacturing Technology, Part C, 18(2), pp. 292–298 (1995).
48. D. Klosterman, L. Li, and J.E. Morris, Materials characterization, conduction development, and curing effects on reliability of isotropically conductive adhesives, IEEE Transactions on Components, Packaging, and Manufacturing Technology, Part A, 21(1), pp. 23–31 (1998).
49. D. Lu, Q.K. Tong, and C.P. Wong, Conductivity mechanisms of isotropic conductive adhesives (ICAs), IEEE Transactions on Electronics Packaging Manufacturing, 22(3), pp. 223–227 (1999).
50. J.C. Jagt, Reliability of electrically conductive adhesive joints for surface mount applications: a summary of the state of the art, IEEE Transactions on Components, Packaging, and Manufacturing Technology, Part A, 21(2), pp. 215–225 (1998).
51. M.G. Perichaud, J.Y. Deletage, H. Fremont, Y. Danto, C. Faure, and M. Salagorty, Evaluation of conductive adhesives for industrial SMT assembles, 23rd IEEE/CPMT Electronics Manufacturing Technology Symposium, 1998, pp. 377–385.
52. R.C. Campbell, S.E. Smith, and R.L. Dietz, Measurements of adhesive bondline effective thermal conductivity and thermal resistance using the laser flash method, 15th Annual IEEE Semiconductor Thermal Measurement and Management Symposium, 9–11 March, 1999, pp. 83–97.
53. M. Mayer, J. Nicolics, G. Hanreich, and M. Mündlein, Thermal aspects of GaAs power FET attachment using isotropically conductive adhesive, 2nd Int. IEEE Conf. on Polymers and Adhesives in Microelectronics and Photonics, Polytronic 2002, Zalaegerszeg, Hungary, June 23–26, 2002, pp. 38–43.
54. http://www.npl.co.uk/ei/iag/leadfree/propertiespbf.html, Lead-Free Alloy Properties, National Physical Laboratory.
55. D.W. Swanson and L.R. Enlow, Stress effects of epoxy adhesives on ceramic substrates and magnetics, Microelectronics Reliability, 41(4), pp. 499–510 (2001).
56. J. Vanfleteren, A. Vervaet, and A.V. Calster, Highlights of the DACTEL project: development of adhesive chip technologies for dedicated electronic applications, Proc. of 23rd Int. Spring Seminar on Electronics Technology, ISSE 2000, Balatonfüred, HU, May 6–10, 2000, pp. 315–318.
57. M. Sumikawa, T. Sato, C. Yoshioka, and T. Nukii, Reliability of soldered joints in CSPs of various designs and mounting conditions, IEEE Transactions on Components and Packaging Technology, 24(2), pp. 293–299 (2001).
58. R. Prasad, Adhesives and its applications, in G.R. Blackwell, Ed., The Electronic Packaging Handbook, CRC Press, IEEE Press, 2000, pp. 10-1–10-28.
59. M. Mündlein, G. Hanreich, and J. Nicolics, Application of an ICA for the production of a radiation sensor, Proc. of 3rd Int. IEEE Conf. on Polymers and Adhesives in Microelectronics and Photonics, Polytronic 2003, Montreux, Schweiz, October 21–23, 2003, pp. 123–127.
60. M. Mündlein, J. Nicolics, and M. Brandl, Packaging concept for a miniaturized wirelessly interrogable temperature logger, Proceedings of the 27th Int. Spring Seminar on Electronics Technology, Sofia, Bulgaria, May 14–16, 2004, pp. 68–73.